**█Anticancer Agents** |*Hot Paper*|

# Towards Identification of Essential Structural Elements of Organoruthenium(II)-Pyrithionato Complexes for Anticancer Activity

Jerneja Kladnik,[a] Jakob Kljun,[a] Hilke Burmeister,[b] Ingo Ott,[b] Isolda Romero-Canelón,[c] and Iztok Turel*[a]

**Abstract:** An organoruthenium(II) complex with pyrithione (2-mercaptopyridine *N*-oxide) **1a** has previously been identified by our group as a compound with promising anticancer potential without cytotoxicity towards non-cancerous cells. To expand the rather limited research on compounds of this type, an array of novel chlorido and 1,3,5-triaza-7-phosphaadamantane (pta) organoruthenium(II) complexes with methyl-substituted pyrithiones has been prepared. After thorough investigation of the aqueous stability of these complexes, their modes of action have been elucidated at the cellular level. Minor structural alterations in the rutheni- um-pyrithionato compounds resulted in fine-tuning of their cytotoxicities. The best performing compounds, **1b** and **2b**, with a chlorido or pta ligand bound to ruthenium, respectively, and a methyl group at the 3-position of the pyrithione scaffold, have been further investigated. Both compounds trigger early apoptosis, induce the generation of reactive oxygen species and G1 arrest in A549 cancer cells, and show no strong interaction with DNA. However, only **1b** also inhibits thioredoxin reductase. Wound healing assays and mitochondrial function evaluation have revealed differences between these two compounds at the cellular level.

## Introduction

The serendipitous discovery of the anticancer activity of cisplatin, *cis*-[PtCl$_2$(NH$_3$)$_2$], in the 1960s[1] and its subsequent introduction in clinical use for cancer therapy in the next decade has led to increased interest in the development of new metallopharmaceuticals.[2] Despite the great efficacy of platinum-based oncotherapeutics, their application can be hindered by severe side effects and the development of drug resistance. Therefore, there is an urgent demand for the discovery of new drugs. Currently, a lot of hope is pinned on two anticancer ruthenium compounds, KP-1339 (also named NKP-1339 or IT-139) and TLD-1433 (Figure 1 A, B), which have entered clinical trials and have shown encouraging outcomes.[3] Besides, ruthenium(II)-arene-pta (RAPTA) complexes, for example, RAPTA-C (Figure 1 C), have shown very promising in vitro and in vivo results[4] and many other ruthenium compounds are being ex-
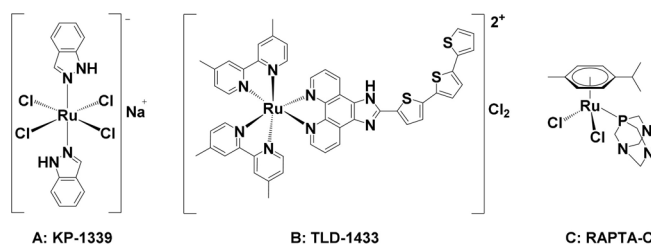


**Figure 1.** Examples of ruthenium-based therapeutic agents with prospective anticancer properties.

plored at the preclinical stage.[5] In recent decades, a lot of research has been focused on the synthesis of new potential organoruthenium(II)-arene anticancer compounds with piano-stool conformation with various chelating ligands, especially *N,N*-, *N,O*-, and *O,O*-donors, which display interesting biological properties.[6] Some organoruthenium(II)-arene complexes with *O,S*-ligands have also been synthesized, albeit to a lesser extent.[7]

Pyrithione (Figure 2 a) is a cyclic thiohydroxamic acid,[8] which exists in solution in two tautomeric forms, predominantly as *N*-hydroxypyridine-2-thione, along with a minor tautomer 2-mercaptopyridine-*N*-oxide.[9] In the solid state, it adopts the thione form.[10] Pyrithione can bind to different metals through its O and S atoms. Zinc pyrithione complex displays very good antimicrobial activity and is widely used as an active ingredient in commercial antidandruff shampoos and as a biocide in antifouling paints.[11] Furthermore, iron, gallium, and bismuth pyrithione complexes are good antibacterial inhibitors against *My-*

[a] J. Kladnik, Dr. J. Kljun, Prof. Dr. I. Turel
Faculty of Chemistry and Chemical Technology
University of Ljubljana, Večna pot 113, 1000 Ljubljana (Slovenia)
E-mail: Iztok.Turel@fkkt.uni-lj.si

[b] H. Burmeister, Prof. Dr. I. Ott
Institute of Medicinal and Pharmaceutical Chemistry
Technische Universität Braunschweig, 38106 Braunschweig (Germany)

[c] Dr. I. Romero-Canelón
School of Pharmacy, Institute of Clinical Sciences
University of Birmingham, Birmingham B15 2TT (UK)

📟 Supporting information and the ORCID identification number(s) for the author(s) of this article can be found under:
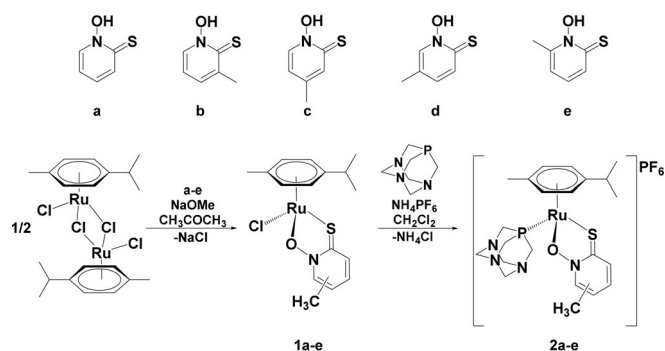https://doi.org/10.1002/chem.201903109.

These are not the final page numbers! ↗↗

**Figure 2.** Structures of the prepared ligands and reaction path leading to the organoruthenium(II) chlorido (**1a**–**e**) and pta (**2a**–**e**) complexes.

*cobacterium tuberculosis*,[12] platinum and palladium complexes show high antiparasitic activity towards *Trypanosoma cruzi*,[13] vanadyl pyrithione displays antidiabetic effects,[14] and nickel,[15] tin,[16] and rhenium pyrithione complexes display anticancer properties.[17]

Recently, our research group was the first to report the synthesis of two $\eta^6$-*p*-cymene and two trithiacyclononane ruthenium(II) coordination compounds with pyrithione and its *O,O*-analogue, with the aim of studying their anticancer activities. Interestingly, complexes with the *O,O*-analogue were found to induce proliferation of the MCF-7 breast cancer cell line, whereas the *O,S*-analogue **1a** (Figure 2) showed a low EC$_{50}$ value (3.81 ± 0.06 μM) along with potent inhibition of overexpressed aldo-keto reductase 1C enzymes (AKR1Cs).[18] Similar observations were noted in the case of hydroxy(thio)pyr(id)one complexes, whereby *O,S*-derivatives displayed better biological activity than the parent hydroxypyr(id)ones, which was attributed to the lower stability of the oxygen-containing counterparts.[19] We also previously reported **1a** as being the only complex among seventeen tested *N,N*-, *N,O*-, *O,O*-, and *O,S*-organoruthenium(II) compounds to display an inhibitory effect towards glutathione *S*-transferase (GST), the key enzyme implicated in the development of drug resistance in cancer treatment (IC$_{50}$ = 2.26 ± 0.5 μM and IC$_{50}$ = 45 ± 5.2 μM for GST from horse serum and human placenta, respectively). It was also proven that **1a** is not cytotoxic at pharmaceutically relevant concentrations against non-cancerous cell types, such as the HUVEC cell line or primary human keratinocytes (NHEK-1). Moreover, while **1a** shows moderate inhibitory potency towards acetylcholinesterase and butyrylcholinesterase, target enzymes for treating Alzheimer's disease, it shows no undesirable side effects on the neuromuscular system at pharmacological concentrations.[20]

Complex **1a**, with all of the abovementioned attractive anticancer characteristics, thus represents our lead compound for further research. Therefore, the aim of this study was fine-tuning of the physicochemical and biological properties by introducing minor structural changes to the lead compound **1a** to gain insight into the structural elements of complexes that are important for anticancer activity and need to be taken into account when planning further lead compound optimization. The synthesis of pyrithione (Figure 2a) and its methyl-substi-

tuted analogues **b**–**e** (Figure 2) was first reported in 1950, and these sulfur analogues of the antibiotic aspergillic acid were found to show high in vitro antibacterial activity.[8] Cohen et al. showed that methyl groups in various positions on pyrithione exert a significant effect on the affinity in a metalloenzyme active site of human carbonic anhydrase II (hCAII).[21] The same group proceeded to prepare 21 more pyrithione analogues and further studied the structure–activity relationship of metal-binding pharmacophores.[22]

With these data in hand, we decided to prepare an array of ten organoruthenium(II) chlorido (**1a**–**e**) and pta (**2a**–**e**) complexes (Figure 2). After an in-depth study of their stabilities under biologically relevant conditions, all compounds were screened for their cytotoxicities against seven cancer cell lines and IC$_{50}$ values were determined. The best-performing pair, namely **1b** and **2b**, was selected for further testing against one normal cell line, and their mode of action was assessed through wound healing assay, binding to bovine serum albumin (BSA), induction of apoptosis, cell cycle analysis, DNA interactions, generation of reactive oxygen species (ROS), inhibition of the potential molecular target thioredoxin reductase (TrxR), and mitochondrial function assay.

## Results and Discussion

### Synthesis

Pyrithione analogues **b**–**e** were synthesized according to the reported procedure (Figure S1, Supplementary Information),[21] and organoruthenium(II) chlorido (**1b**–**e**) and pta (**2a**–**e**) complexes were newly prepared through two-step syntheses (Figure 2).

Neutral chlorido complexes **1a**–**e** were prepared according to a previously reported procedure for **1a** with some modifications.[18] The reaction mixture in acetone was stirred overnight at room temperature. Sodium methoxide was used as a base to deprotonate the relevant ligand, and NaCl precipitated out as a by-product. Deprotonation of the thiohydroxamic group allows the ligands to bind to the metal centre through their S and O atoms. The solvent was evaporated after 24 h and the chlorido complexes were purified by column chromatography on silica gel (mobile phase 5% CH$_2$Cl$_2$/acetone) to remove traces of unreacted ligands and precipitated NaCl. For the precipitation of all complexes, a CH$_2$Cl$_2$/heptane solvent/antisolvent combination was used. After filtration under reduced pressure, red solids were obtained, which proved to be light, air, and moisture stable.

From the literature, it is known that organoruthenium(II) complexes with halides are prone to exchange their labile halido ligand with water as a first step of hydrolysis, form aqueous species, and thus act as prodrugs.[23] In order to evaluate the importance and the effect of the aquation step on the mode of action and efficacy of the novel compounds, we synthesized a second series of organoruthenium(II) complexes **2a**–**e**, in which the chlorido ligand in the series **1** complexes is substituted by a 1,3,5-triaza-7-phosphaadamantane (pta) neutral ligand. According to our research paper on organoruthe-

**↖↖ These are not the final page numbers!**

nium(II)-diketonato complexes[24] and data from other research groups,[25] the monodentate pta ligand seemingly slows down the hydrolysis rate and frequently increases the aqueous solubility of the complexes. Complexes **2a–e** were synthesized in $CH_2Cl_2$ and stirred over two nights in the dark to prevent decomposition. Chloride anion abstraction through the addition of $NH_4PF_6$ enables the binding of pta to ruthenium through the phosphorus atom, with the precipitation of $NH_4Cl$ as a white salt. Importantly, to increase yields, pta needs to be ground to a fine white powder in an agate mortar as it is only sparingly soluble in $CH_2Cl_2$. After completion of the reaction, the reaction mixture was concentrated by using a rotary evaporator and precipitated $NH_4Cl$, unreacted $NH_4PF_6$, and pta were filtered off through Celite. The mother liquor was further concentrated, and heptane was added to precipitate the product. However, during optimization, cold diethyl ether proved to be a better antisolvent choice. The precipitates were left to stand in a refrigerator for around 10 min, and then collected by filtration under reduced pressure as yellow-orange solids. Although we have not noticed any visible changes after precipitation of the pta complexes under ambient conditions, all pta complexes were stored in a desiccator protected from direct light exposure to prevent any possible decomposition, as previously reported for similar systems.[26]

### Crystal structure determinations

Crystal structures were obtained for four ligands and three chlorido and five pta organoruthenium(II) complexes (Figure 3; Figures S2–S4 and Tables S1–S3, Supplementary Information). Crystals of ligands **b**, **c**, **d**, and **e** were obtained by solvent diffusion from $CH_2Cl_2/n$-heptane or $CH_2Cl_2/n$-hexane. The crystal structure of **1a** crystallized from $CH_2Cl_2/n$-hexane has been previously reported.[18] Complexes **1b**, **1c**, and **1e** were crystallized by a vapour diffusion method from a solvent system of $CHCl_3/n$-heptane. Compounds **2a** and **2c** crystallized from $CH_2Cl_2/n$-hexane by solvent diffusion; crystals of **2b**, **2d**, and **2e** were obtained from the same solvent system, but by vapour diffusion. All compounds crystallized at ambient temperature, except for **2c**, which crystallized at 4 °C.
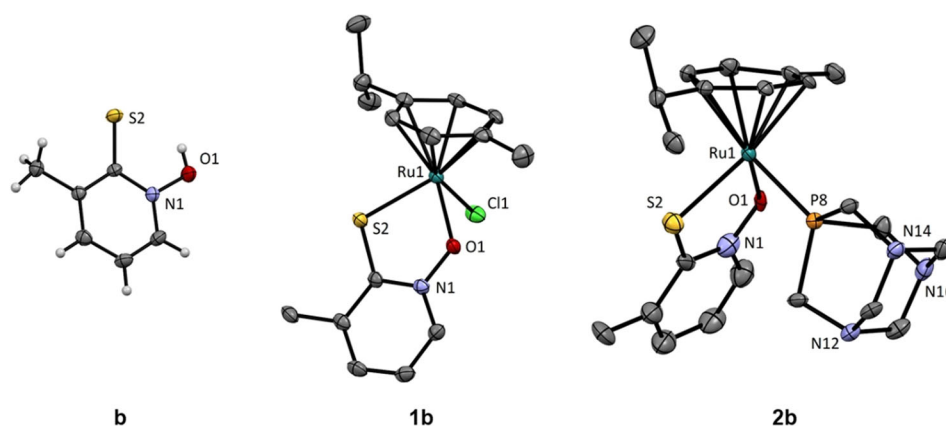
Crystal structures showed that in solid state all ligands exist as the *N*-hydroxy-2-thione tautomers. The organoruthenium(II) complexes have pseudo-octahedral geometry, with three coordination sites being occupied by the π-bound cymene ligand. The pyrithionato ligands are all bound in deprotonated form through the O1 and S2 atoms, and the remaining site is occupied by the chlorido ligand in the series **1** compounds and by the phosphorus ligand pta in the series **2** compounds. The cationic structure of the series **2** compounds is counterbalanced by a hexafluorophosphate ion. Due to the minor nature of the structural modifications, the bond distances and angles do not differ significantly from those in the previously reported parent structure.[18]

### UV/Vis aqueous stability

Before conducting biological assays, it is important to assess the stabilities of the tested compounds. Therefore, the stability of the complexes was investigated by UV/Vis and ^{1}H and ^{31}P NMR spectroscopy at room temperature in different aqueous media. The conditions for these experiments aimed to mimic those used to perform cytotoxicity assays on different cell lines. Hence, stock solutions of all complexes were prepared using 100% DMSO, which were then diluted in biologically relevant matrixes to achieve working concentrations. The resulting working solution at 200 μM matched the highest concentration used for cell viability tests. Single-beam UV/Vis scans were performed between 250 and 900 nm within 5 min of sample preparation and again after incubation for 24 h at 37 °C in the dark in sealed cuvettes. The chosen matrices included water, phosphate-buffered saline (PBS), Roswell Park Memorial Institute 1640 cell culture medium (RPMI-1640), fully prepared RPMI-1640 to which 10% (v/v) fetal calf serum and 1% (v/v) penicillin/streptomycin antibiotics had been added, and human blood plasma (UV/Vis spectra for **1b** and **2b** are presented in the Supplementary Information, Figures S5 and S6).

UV/Vis spectroscopy of metal-based complexes allows determination of changes in the metal coordination sphere by the observation of spectral modifications. Hence, it is highly useful to establish the stability of a complex in a given matrix



**Figure 3.** Crystal structures of selected compounds: ligand **b**, and the chlorido **1b** and pta **2b** complexes. Thermal ellipsoids are drawn at the 35% probability level. In the structures of **1b** and **2b**, hydrogen atoms are omitted for clarity. In the structure of **2b**, the $PF_6^-$ anion is also omitted.

These are not the final page numbers! ↗↗

through comparison between spectra at two time points. In particular, the relationship between the results of water and PBS stability tests allows the detection of hydrolysis and its suppression by excess NaCl. Hydrolysis is often associated with metal-drug activation. The investigated chlorido and pta complexes all proved to be stable in the studied matrices under the described conditions.

Similarly, investigations in RPMI-1640 and, most importantly, in fully prepared cell culture medium, showed general complex stability, which indicated that all chlorido and pta derivatives remained chemically unchanged under the conditions and in the timeframe used for biological activity experiments. Pertinently, this suggests that the complexes do not interact with the fetal calf serum included in the fully prepared cell culture medium. Such interaction could potentially alter the cellular accumulation of a given complex during cell-based assays. The final matrix to be investigated was human blood plasma, which is highly relevant when considering the development of a chemotherapeutic agent that would be administered intravenously. All of the tested complexes proved to be stable under the described conditions. It is worth highlighting that human plasma has a chloride concentration of 140 mM and a high albumin content, and so results obtained in this matrix (taken together with those in PBS) are highly relevant. Our findings suggest that the complexes would remain chemically stable when in systemic circulation, and that any interactions with albumin do not include covalent binding to the metal centre, which may be beneficial for transport and distribution of the drug. To further evaluate the interaction of complexes with bovine serum albumin (BSA), a protein-binding study was also conducted to confirm the above results.

### NMR aqueous stability

The stability of the tested compounds was also investigated by $^1H$ and $^{31}P$ NMR spectroscopy to follow any possible structural changes. Spectra were recorded in 5% [$D_6$]DMSO/$D_2O$ and in 5% [$D_6$]DMSO/$D_2O$ containing 140 mM NaCl to evaluate the influence of chloride, which is present at the same concentration in human plasma. Approximately 4 mg of **1b** or **2b** was first dissolved in [$D_6$]DMSO to facilitate dissolution, and $D_2O$ or $D_2O$ containing NaCl was added to obtain 600 μL of 5% [$D_6$]DMSO/$D_2O$ solutions. Spectra were recorded immediately after the preparation and later at different time points. Complex **1b** proved to be very stable in both investigated media (Figures S7 and S8, Supplementary Information), in agreement with our previous report of the stability of **1a**.[18] The first very small peaks of free p-cymene appeared after one day at $\delta \approx 7.2$ ppm and after twelve days at $\delta \approx 6.7$ ppm. Chlorido complexes thus show favourable stability for the timeframes of the conducted biological assays, which included 24 h drug exposure for $IC_{50}$ determinations and 24 h or less for the determination of mechanism of action assays.

Furthermore, the stability of complex **2b** was examined to evaluate the effect of the replacement of the chlorido ligand by pta (Figures S9–S12, Supplementary Information). The initial changes in the NMR spectra in both media, though very small, appeared after 3 h in the aromatic region at $\delta \approx 7.2$ ppm, when p-cymene starts to dissociate from the ruthenium species. Furthermore, after 2 days, an additional small peak appeared at $\delta \approx 6.7$ ppm, also corresponding to a free arene ring, consistent with the data for our organoruthenium(II) complexes with pta and O,O-ligands.[24] In 5% [$D_6$]DMSO/$D_2O$, small peaks appeared after one day in the region corresponding to the pta protons at $\delta \approx 4.4$–4.0 ppm, which surprisingly correspond to the uncoordinated oxidized pta (ptao; 1,3,5-triaza-7-phosphaadamantane 7-oxide). A similar observation has been reported for RAPTA-type complexes with strongly electron-withdrawing arene ligands.[27] When the stability of **2b** was followed in 5% [$D_6$]DMSO/$D_2O$ containing NaCl, another phosphorus species was observed, although in a minor share. Overall, when comparing the spectra, fewer structural changes are observed in media containing NaCl. Considering these changes, NMR stability data are in good agreement with the obtained UV/Vis results, both of which are adequate for performing biological assays within an appropriate timespan, as the complexes are sufficiently stable in the timeframe of biological experiments.

### Cytotoxicity assays: determination of $IC_{50}$ values

Ten organoruthenium(II) compounds were evaluated against seven different cell lines, namely A549 lung, HCT116 colon, OE19 oesophageal, SKOV3 ovarian, HEPG2 hepatocellular, SW626 ovarian, and PC3 prostate cancer cells (Table 1). In general, the complexes showed good anticancer activity in the low micromolar range against all of the tested cell lines. Remarkably, the best performances of the complexes were observed against cell lines A549 and HCT116 of lung and colon

**Table 1.** Antiproliferative activities of the prepared compounds towards different cancer cell lines.

| | $IC_{50}$ values (μM) towards different cell lines[a] | | | | | | |
| | A549 | HCT116 | OE19 | SKOV3 | HEPG2 | SW626 | PC3 |
|---|---|---|---|---|---|---|---|
| **1a** | 3.6±0.3 | 14.1±0.4 | 11.2±0.3 | 7.5±0.6 | 24.4±0.4 | 27.8±0.3 | 22.8±0.3 |
| **2a** | 3.7±0.3 | 13.7±0.2 | 12.4±0.3 | 9.2±0.3 | 22.1±0.9 | 30.4±0.7 | 20.8±0.2 |
| **1b** | <u>1.86±0.08</u> | <u>2.4±0.3</u> | <u>4.0±0.2</u> | <u>4.7±0.3</u> | <u>8.3±0.4</u> | <u>10.4±0.7</u> | <u>12.8±0.9</u> |
| **2b** | <u>2.21±0.09</u> | <u>3.13±0.08</u> | <u>3.95±0.08</u> | <u>3.8±0.7</u> | <u>7.9±0.4</u> | <u>9.4±0.2</u> | <u>10.5±0.5</u> |
| **1c** | 4.84±0.07 | inactive[b] | <u>10.3±0.5</u> | 14.6±0.3 | <u>18.6±0.7</u> | 32.6±0.9 | inactive[b] |
| **2c** | 8.3±0.4 | inactive[b] | 12.6±0.7 | inactive[b] | <u>19.1±0.8</u> | <u>21.2±0.1</u> | 25.8±0.6 |
| **1d** | <u>2.13±0.09</u> | <u>6.3±0.5</u> | <u>9.2±0.3</u> | <u>6.8±0.4</u> | <u>16.6±0.5</u> | <u>19.3±0.2</u> | <u>17.5±0.9</u> |
| **2d** | 5.32±0.06 | <u>5.4±0.3</u> | <u>10.4±0.6</u> | <u>7.5±0.3</u> | <u>13.1±0.6</u> | <u>22.6±0.3</u> | <u>15.4±0.6</u> |
| **1e** | 6.4±0.2 | <u>10.5±0.7</u> | <u>7.5±0.3</u> | 12.6±0.4 | <u>12.5±0.6</u> | <u>15.3±0.2</u> | <u>16.8±0.3</u> |
| **2e** | 7.7±0.2 | <u>8.8±0.2</u> | <u>8.1±0.4</u> | 13.5±0.6 | <u>21.4±0.3</u> | <u>16.1±0.9</u> | <u>16.1±0.7</u> |

[a] Mean $IC_{50}$ values with standard deviations determined as duplicates of triplicates in two independent sets of experiments. Values indicating better activity of the complexes than our lead complexes **1a/2a** are underlined. [b] Compounds considered inactive have $IC_{50}$ values above 150 μM under the following experimental conditions: 24 h drug exposure and 72 h recovery time in drug-free medium, with 200 μM as the maximum concentration tested.

↖↖ **These are not the final page numbers!**

origin, while the highest IC$_{50}$ values were obtained against SW626 and PC3 lines of ovarian and prostate origin, with an approximate order of magnitude difference in potency between the former and the latter set of cell lines.

Comparison of the IC$_{50}$ values of the complexes against a single cell line indicates that our structural variations (i.e., the position of the methyl group) do alter their anticancer activities, and we were able to establish a preliminary structure–activity relationship. By changing the position of a single methyl substituent on the pyrithione scaffold, the anticancer activities of the complexes towards different cell lines are improved or diminished in comparison to our lead compound **1a**. Complexes **1b** and **2b**, with a methyl group in the 3-position, performed better against all tested cell lines (Table 1, underlined and bold values) compared to unsubstituted pyrithione complexes **1a** and **2a**. The same pattern was observed for ruthenium complexes **1d** and **2d**, except in one case (**2d** appeared less active towards the A549 cell line). Ligands **b** and **d** both bear methyl substituents at positions at which electron density can be donated to sulfur, and may thereby stabilize its binding to the ruthenium centre. Nevertheless, **1b** and **2b** show higher anticancer activities against all cell lines than **1d** and **2d**. The activities of the complexes towards some cell lines are further reduced by placing the methyl substituent in other positions. Remarkably, complexes **1c** and **2c**, with a methyl substituent in the 4-position on the pyrithione scaffold, even proved to be inactive towards HCT116, SKOV3, and PC3 cells. Regarding the substitution of chlorido by a pta ligand, the IC$_{50}$ values are comparable, though the chlorido complexes generally show better anticancer activity towards A549, OE19, SKOV3, and SW626 cell lines, whereas the pta analogues show better activity towards the HCT116, HEPG2, and PC3 cell lines. This anticancer activity screening was conducted with the aim of gaining insight into where structural changes should be made in subsequent optimization. The collected results indicate that cytotoxicity can be somewhat improved by introducing small structural changes. In our case, it was established that introducing a methyl substituent at the 3-position of the pyrithionato scaffold makes complexes **1b** and **2b** the best performing compounds against all cell lines among all tested complexes, and that the electron-donating group needs to be placed at a position at which it can increase the electron density on sulfur. The activities of complexes **1b** and **2b** were highest against the A549 lung cancer cells, and in view of these results, further investigations were focused on these complexes and the A549 cell line in order to establish their mechanism of action at the cellular level.

### Cancer cell selectivity

Complexes **1b** and **2b** were further tested towards MRC5 lung fibroblasts (Table 2). This experiment allowed the determination of selectivity factors, defined as the ratio between the IC$_{50}$ values obtained against the normal cell line and the corresponding values against A549 cancer cells. This gives an indication of the preferential toxicity of the complexes towards cancer cells. Notably, both metal complexes proved to be less

**Table 2.** IC$_{50}$ values of the selected compounds towards A549 lung cancer and MRC5 normal cell lines and their selectivity factors.

| Compound | IC$_{50}$ values ($\mu$M)[a] | | Selectivity factor[b] |
|---|---|---|---|
| | A549 | MRC5 | |
| **1b** | 1.86 $\pm$ 0.08 | 8.75 $\pm$ 0.09 | 4.70[c] |
| **2b** | 2.21 $\pm$ 0.09 | 9.1 $\pm$ 0.6 | 4.11[c] |
| Cisplatin | 3.5 $\pm$ 0.2 | 11.5 $\pm$ 0.4 | 3.28 |

[a] Mean IC$_{50}$ values with standard deviations determined as duplicates of triplicates in two independent sets of experiments. [b] Selectivity factors defined as the ratio between the IC$_{50}$ value in MRC5 normal fibroblasts divided by the corresponding value in A549 cancer cells. [c] Selectivity factors superior to that of cisplatin are underlined.

toxic towards MRC5 and showed improved selectivity factors compared to that of cisplatin under similar experimental conditions.

### Wound healing assay

We further explored how exposure to complexes **1b** and **2b** affects the migration of A549 cancer cells. During this assay, a gap or a wound is generated in a cellular monolayer and the rate of cell growth towards closing the gap is measured and compared between untreated controls and cells exposed to the metal complexes (Figure S13 and Table S4, Supplementary Information). Untreated cells were able to close 75.1% of the gap within 24 h, whereas the complexes showed a concentration-dependent effect on wound recovery. Although at 2 $\mu$M the results with complex **1b** were comparable to that with the untreated control (76.5%), at 4 $\mu$M the closing percentage was reduced to 44.7%. For complex **2b**, the values were reduced to 30.4% and 19.2% at 2 $\mu$M and 4 $\mu$M, respectively. This assay gave a first indication that small modifications in the structures of both metal complexes could have a great effect on their cellular behaviour, beyond their activity expressed in terms of IC$_{50}$ values.

### Protein binding studies

The above-described properties of the tested compounds imply very favourable anticancer effects. However, the positive pharmacological effect of a drug is only possible if it reaches its target in sufficient concentration. Albumin is the most abundant serum protein in blood and can bind enormous numbers of drugs, thereby also acting as a delivery system. Nonetheless, at the site of action, only the unbound form of the drug can induce pharmacological effects.[34] UV/Vis stability data for the complexes in human plasma showed very convenient properties, which were additionally confirmed by a protein binding study conducted with **1b** and **2b** on bovine serum albumin (BSA). Measurements were made at time point 0 and after 1 h at a complex concentration of 3 $\mu$M. The results showed that initially 81% ($\pm$0.01) of complex **1b** was bound to BSA, falling to 71% ($\pm$0.1) after 1 h. In the case of **2b**, initially only a small amount of the pta complex was bound to BSA (6% $\pm$0.1). However, after 1 h, the amount of bound **2b**

increased to 58% ($\pm0.04$). The higher reactivity of **1b** compared to **2b** is certainly related to the fact that the chlorido ligand of **1b** is a better leaving group than the pta ligand of **2b**. From the obtained data, we can conclude that albumin could serve as a possible transporter for our complexes. Besides, the compounds also exist in their unbound form and as such can interact with therapeutic targets.

### Induction of apoptosis

The induction of programmed cell death by complexes **1b** and **2b** was investigated in A549 lung cancer cells after 24 h of drug exposure. This timeframe was set to coincide with the drug exposure time used for the determination of IC$_{50}$ values. Flow cytometry analysis takes advantage of cells that are doubly-stained with Annexin V-FITC and propidium iodide (PI). In a two-dimensional analysis, cells that are singly- or doubly-stained can be allocated into four subgroups: a) viable cells showing low fluorescence in both flow cytometry channels, b) early apoptotic cells labelled only with Annexin after loss of symmetry in the phospholipid membrane, c) late apoptotic cells that exhibit high fluorescence in both channels, and d) non-viable cells that have become permeant to PI.

In these experiments, untreated controls showed a majority of the cellular population in the first (a) subgroup (98%) (Figure 4a; Table S5, Supplementary Information). In comparison, complexes **1b** and **2b** statistically increased the populations in the early apoptotic group (b) in a concentration-dependent

manner. Remarkably, in neither case was there any significant change in late apoptotic or non-viable cell population sets. This indicated that the cell death mechanisms, activated by the organoruthenium(II) complexes **1b** and **2b**, were triggered within 24 h of drug exposure, but their final effects were only observed after the recovery time was included in the experiments to determine IC$_{50}$ values (72 h). This is consistent with optical microscopy observation of A549 cells exposed to complexes **1b** and **2b**, which showed no significant reductions in cell population after 24 h (Figure S14, Supplementary Information). The observed induction of early apoptosis does not rule out the involvement of parallel mechanisms of cell death. In fact, metal-based complexes, which are frequently multi-targeted, can often induce multiple mechanisms of action.

### Cell cycle analysis

The influence of complexes **1b** and **2b** on the cell cycle of A549 lung cancer cells was further evaluated by flow cytometry employing drug-exposed cells stained with PI after ethanol fixation. This experiment allowed the detection of cellular populations in the G1, G2/M, and S phases of the cell cycle. G1 and G2 are growth phases separated by the S phase, in which DNA is synthesized, and the M phase, during which mitosis occurs.[28] Cell cycle profiles were obtained by measuring the fluorescence intensity of PI in the FL2 red channel as a reflection of quantitative DNA binding. The analysis used two concentrations of the organoruthenium(II) complexes and the results were compared with those of untreated controls. As expected, the negative controls showed the highest population percentages in the G1 phase, followed by approximately equal populations in the G2/M and S phases (Figure 4b; Table S6, Supplementary Information). Samples exposed to chlorido complex **1b** showed a concentration-dependent G1 arrest, with its population increasing from 61% to 73 and 79%. This G1 arrest was accompanied by reductions in the populations in the G2/M and S phases. Similar results were obtained for complex **2b**, in case of which G1 populations increased to 70 and 72%. The lower arrest caused by the pta derivative **2b** could be correlated with the slightly reduced activity of this complex in comparison to the chlorido analogue. In both cases, cellular arrest in the G1 phase highlights the potential cytostatic activity of the respective complexes as part of their multi-targeted mechanism of action, and further indicates that they are less likely to rely on DNA interactions as a part of their cellular anticancer behaviour. Such activity would be observed with a cell cycle arrest similar to that with cisplatin in the S phase. This opens the possibility of exploiting the investigated complexes to overcome platinum resistance, which is a well-established clinical need. Compounds that incorporate metals other than platinum may have different modes of action and/or toxicity profiles, and may therefore offer new opportunities in combating resistance and/or the side effects of platinum drugs.[29]
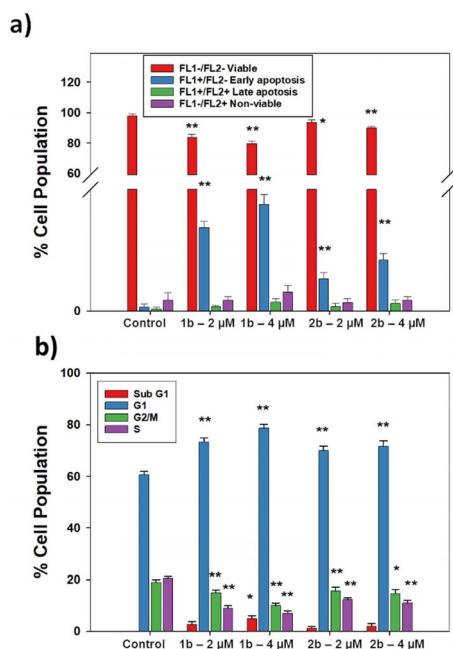


**Figure 4.** Flow cytometry investigations of A549 cancer cells exposed to complexes **1b** and **2b** for 24 h at 2 and 4 μM. Bar charts show the average percentage cell population present in each category in triplicate samples ($p < 0.01$ for **, and $p < 0.05$ for *). a) Induction of apoptosis and b) cell cycle analysis. Samples recorded by reading Annexin V-FITC in the FL-1 green channel and propidium iodide in the FL-2 red channel; data processed using Flowjo.

## DNA interactions

Given the results obtained in the cell cycle analysis of A549 cells exposed to complexes **1 b** and **2 b**, we decided to confirm that the test-tube interactions of both complexes with calf thymus DNA (CT-DNA) were negligible. In a first experiment, buffered solutions of CT-DNA and various concentrations of the metal complexes were incubated at 37 °C and re-evaluated after 24 h. Comparing the results obtained between 0 h and 24 h, together with comparisons against metal-complex-only solutions, we were able to determine that there were no variations in the charge-transfer bands for any of the complexes at any of the concentration ratios measured (Figures S15 and S16, Supplementary Information). A shift in wavelength or hypo/hyperchromism for such bands would be expected upon DNA–complex interaction. A second experiment included evaluation of the CT-DNA melting temperature in a buffered solution compared to samples that comprised a mixture of CT-DNA and the metal complexes. DNA melting point refers to the temperature at which an equilibrium between single- and double-stranded DNA is established, and perturbations of this value would indicate that the complexes are capable of disrupting or stabilizing the DNA double-helix. No changes in melting temperature were detected, with both the CT-DNA and the mixtures of CT-DNA/complexes melting at approximately 66 °C (Table S7, Supplementary Information). These results were consistent with the previous observation that the cell cycles of A549 cells exposed to complexes **1 b** and **2 b** were not arrested in the S phase.

## Induction of reactive oxygen species (ROS)

A balanced redox state in the cell is crucial for maintaining diverse cellular functions,[30] and organometallic complexes are often reported to be involved in ROS generation in intracellular space.[31] Such activity may be linked to their mode of action, particularly taking into account the high likelihood of metal complexes acting on multiple targets simultaneously.[30] Hence, ROS induction, initiated by exposure to compounds **1 b** and **2 b**, was investigated to assess the effect of the tested compounds in A549 lung cancer cells. These experiments included comparisons with the known ROS inducers hydrogen peroxide and luperox. Figure 5 a shows a statistically significant increase in the ROS induction of samples exposed to the complexes with concentration-dependent trends. At each of the concentrations applied, the increment in fluorescence intensity correlates with the increased potency and therefore with the cytotoxicity values determined, with complex **1 b** generating the most ROS, followed by pta complex **2 b** (intensities 0.517 and 0.472, respectively). These observations are consistent with a multi-targeted mechanism of action that involves modulation of the redox state of the cancer cells, as higher cellular ROS concentrations may induce activation of different signalling pathways or damage to cellular components, such as DNA, proteins, or lipid components, leading to apoptosis.[32] Interestingly, zinc pyrithione complex has also been reported to increase ROS levels and induce a death pathway in the PC3 cell
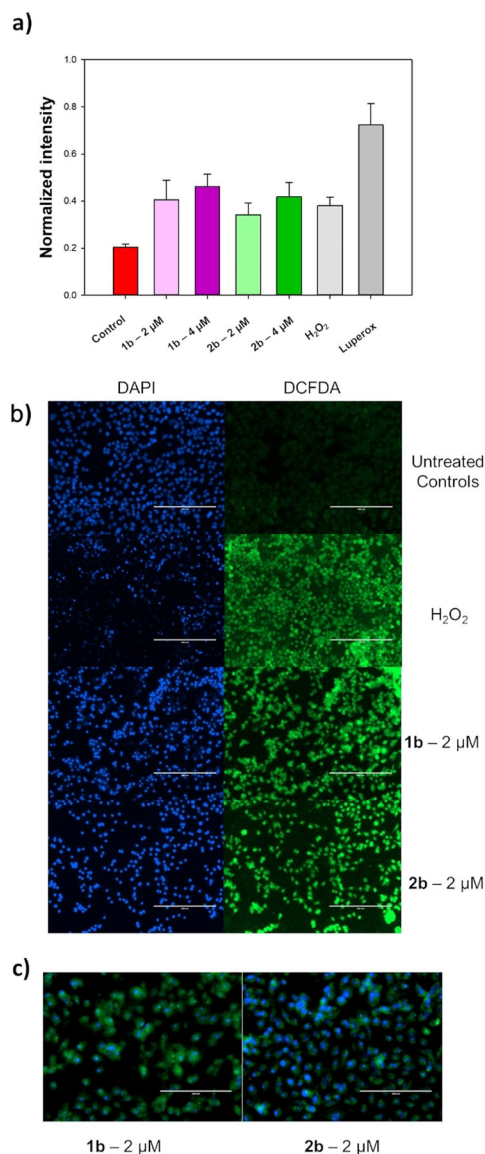


**Figure 5.** ROS induction in A549 cancer cells exposed to complexes **1 b** and **2 b** for 24 h at 2 and 4 μM. a) Bar chart showing quantitative measurements normalized to untreated controls, expressed as the mean ± standard deviations from triplicate samples, b) fluorescence microscopy unmerged channels using DAPI (blue) and DCFDA (green) with 10× magnification, and c) fluorescence microscopy using merged DAPI (blue) and DCFDA (green) channels with 20× magnification.

line.[33] On the other hand, RAPTA-C and its analogues with *O,O*-diketonate ligands show no ROS production.[24] Thus, ROS generation in the case of our pta complex **2 b** probably derives from the ligand. Qualitative fluorescence microscopy results were in accordance with these quantitative results (Figure 5 b, c).

## Thioredoxin reductase inhibition

Considering cancer as one of the most complex diseases, the single-target drug approach seems to fail and it appears that multi-target drugs now pave the way to achieve adequate

therapeutic effects.[29,35] Our lead compound **1a** has already shown good inhibition of AKR1C and glutathione S-transferase, two enzymes involved in cancer progression.[18,20] In the literature, arsenic complexes, including one bearing a pyrithione ligand, have been reported to show a very good ability for inhibiting thioredoxin reductase (TrxR),[36] one of the crucial enzymes that regulates redox homeostasis in cells. If overexpressed, it can also cause cancer progression and the latter thus represents an interesting "druggable" target.[37] The first report on the significant TrxR inhibition by ruthenium(III) complexes appeared in 2007,[38] which prompted further studies with organoruthenium(II) compounds.[39–42] Hence, we decided to conduct preliminary tests on the inhibitory potencies of **1b** and **2b** against TrxR, following an established protocol.[39,40] Chlorido complex **1b** suppressed 45% of enzyme activity at the tested 10 μM concentration compared to a positive control (enzyme not treated with a compound), whereas pta complex **2b** showed no inhibition towards TrxR. From the literature, it is known that metal compounds can promote the death of cancer cells through ROS-mediated apoptosis by targeting TrxR, because the inhibition of TrxR induces accumulation of ROS.[43] Additionally, some Au, Pt, Cr, Hg, As, and Se compounds with anticancer activity show inhibition of TrxR, which results in DNA damage, elevated ROS levels, and cell cycle changes leading to apoptosis.[37] Both greater generation of ROS and higher G1 arrest were observed for complex **1b**, which could be partly correlated with its TrxR inhibition. On the other hand, higher ROS generation and higher G1 arrest were observed for **2b**, which does not inhibit TrxR, but to a lesser extent, probably as a result of other underlying mechanisms. It has also been reported that some neutral Ru(II)-arene pta complexes are modest inhibitors of TrxR, whereas positively charged pta complexes, such as **2b**, induce no significant inhibition.[41] Some organoruthenium(II) complexes with N-heterocyclic carbene (NHC) ligands and a labile halide also reduce the activity of TrxR, but not the NHC ligands themselves.[39,40,44] We were also interested in determining the origin of the inhibition of TrxR of our ruthenium complex **1b**. Therefore, we tested whether ligand **b** alone could influence TrxR activity. No inhibition of this enzyme by ligand **b** was detected. Evidently, binding of the pyrithione-based ligand to the metal centre is essential for the inhibition of TrxR. A halide ligand must also be present for the activity of our organoruthenium(II) complexes. Although complex **1b** does not induce very strong inhibition of the enzyme, our results indicate that TrxR inhibition might be one of several factors that determine the cytotoxicity of the complex. In the context of drug development, identification of targets for biologically active compounds is crucial for understanding the underlying modes of action of the active compounds and for their further optimization. Therefore, further studies to support these findings and to better understand the mechanism of action and possible targets are planned.

### Evaluation of mitochondrial function

Given the results from the ROS induction and the behaviour of complexes **1b** and **2b** against TrxR, we decided to investigate the mitochondrial function of A549 cells exposed to the metal complexes for 24 h. To this end, we stained exposed cells with three fluorescent probes: DAPI, PI, and rhodamine-123 (Rh-123). The first probe enables sample and nuclei localization, PI acts as a marker for cell membrane integrity, and the fluorescence of Rh-123 is indicative of mitochondrial function. The results shown in Figure 6 confirm once more the differences at the cellular level between complexes **1b** and **2b**. The former, which inhibits TrxR, reduces mitochondrial function in a concentration-dependent manner and compromises the cellular membrane only at high potency, whereas the latter causes membrane damage and minimizes mitochondrial function at both concentrations tested. Figure 6 also reveals that the untreated controls do not show red fluorescence (from PI) and exhibit high Rh-123 signals.
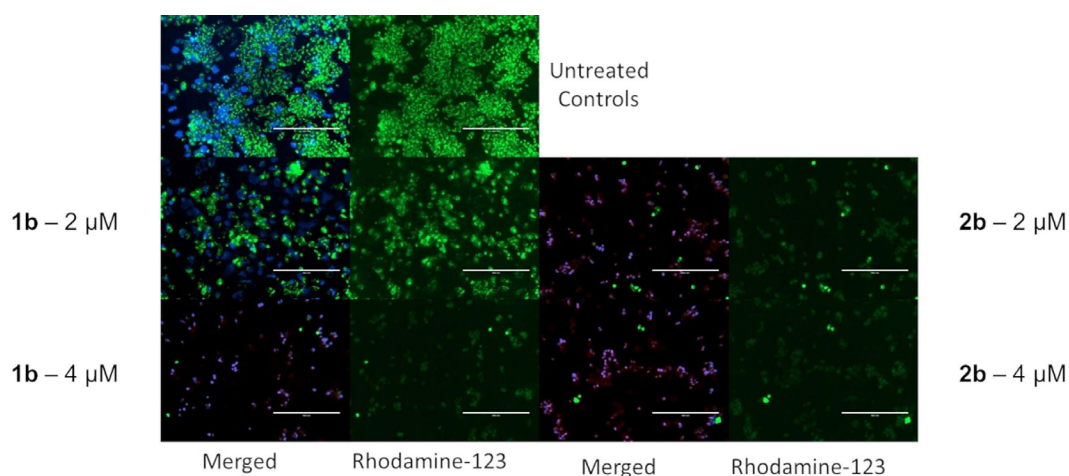


**Figure 6.** Evaluation of mitochondrial function in A549 cancer cells exposed to complexes **1b** and **2b** for 24 h at 2 and 4 μM. Fluorescence microscopy images show unmerged green channel using Rh-123 and merged images including DAPI (blue), propidium iodide (red), and Rh-123 (green), each at 10× magnification.

↖↖ **These are not the final page numbers!**

## Conclusions

A series of novel chlorido and pta organoruthenium(II) complexes with methyl-substituted pyrithiones has been prepared, fully characterized, and examined for their anticancer properties. All compounds show sufficient stability in different aqueous media as well as in human blood plasma for further biological evaluation. Besides, a protein binding study has additionally proven that albumin could act as a potential transporter of the tested complexes. However, because of the reversible binding, the free forms of the compounds are also available at the site of action. The compounds show comparable anticancer activities in a very low micromolar range against cancer cell lines of different origin. Nevertheless, we were able to find some distinguishing patterns to establish preliminary structure–activity relationship. Importantly, complexes with ligands **b** or **d**, bearing a methyl substituent at positions in which it can increase the electron density on sulfur, perform better than the others. Generally, the compounds showed the lowest $IC_{50}$ values towards A549 lung cancer cells, and among all cell lines compounds **1 b** and **2 b** gave the best results. The cytotoxicities of the latter pair towards normal cells imply that binding of the ligand to the metal centre increases selectivity towards cancer cell lines, with compound **1 b** being the least toxic to normal cells. Furthermore, most of the cell death mechanisms of complexes **1 b** and **2 b** are triggered within 24 h, when early apoptotic cells appear. Greater ROS generation as well as higher G1 arrest were also observed with **1 b** and **2 b**. Therefore, unlike cisplatin, with its main target DNA causing S phase arrest, we suggest a multi-target mode of action for our complexes. CT-DNA titrations and melting temperature experiments confirmed no strong interactions between DNA and the tested complexes, consistent with the results of cell cycle analysis causing G1 instead of S arrest. Higher percentages of the cell population in the early apoptotic group as well as in the G1 phase of the cell cycle and higher ROS generation with **1 b** in comparison to **2 b** seem to be mutually associated with TrxR inhibition, which was observed for chlorido complex **1 b**. It has also been proven that ligand **b** itself cannot cause the inhibition of TrxR, whereas when bound to ruthenium it becomes active. Based on these results, the full anticancer potential of pyrithionato compounds is only achieved when an appropriately substituted pyrithione ligand is bound to ruthenium together with a halide ligand. Furthermore, some discrepancies between the chlorido and pta complexes in wound healing and mitochondrial function assays imply different mechanisms of anticancer action at the cellular level. Whereas chlorido complex **1 b** showed concentration-dependent wound recovery and reduced mitochondrial function, the pta complex **2 b** prevented closure of the wound and showed mitochondrial membrane damage at both concentrations tested. Considering the paucity of literature data, this study represents the first in-depth characterization of the anticancer activity of organoruthenium(II)-pyrithionato compounds. Therefore, for future drug development, these findings may aid further rational design and should be taken into consideration when planning new improved anticancer candidates of this type.

## Experimental Section

**Materials and methods**: Ligand **a**, starting materials for the syntheses of ligands **b**–**e**, and other reagents for the syntheses of complexes **1 a**–**e** or **2 a**–**e** were purchased from commercial suppliers (Fluorochem, Strem Chemicals) and were used as received. Phosphine ligand pta was prepared according to the published procedure.[45] For the biological assays, propidium iodide (PI; 94%), RNAse, 2′,7′-dichlorofluorescein diacetate (DCFH-DA), *tert*-butyl hydroperoxide (TBHP), and hydrogen peroxide were purchased from Sigma-Aldrich. Solvents used for the reactions of the complexes were dried over sodium sulfate, whereas solvents used for the isolation of the compounds were used without further purification or drying. Pre-coated TLC sheets ALUGRAM® SIL G/UV$_{254}$ (Macherey–Nagel) were used to follow the progress of the reactions, and were visualized under UV light. Column chromatography was performed on Merck silica gel 60 (35–70 μm) as the stationary phase. NMR spectroscopy was performed on a Bruker Avance III 500 spectrometer at room temperature. $^1$H NMR spectra were recorded at 500 MHz. Chemical shifts are referenced to residual peaks of the deuterated solvent CDCl$_3$, (CD$_3$)$_2$CO, or D$_2$O at 7.26 ppm, 2.05 ppm (referenced to the central line of a quintet), and 4.79 ppm, respectively. $^{31}$P NMR spectra were recorded at 202 MHz and chemical shifts are reported relative to an external standard. The splitting of proton resonances is designated as s = singlet, d = doublet, t = triplet, q = quartet, hept = heptet, m = multiplet, and br = broad signal. Chemical shifts ($\delta$) and coupling constants ($J$) are given in ppm and Hz, respectively. All NMR data were processed using MestRe-Nova version 9.0.1 or 11.0.4. Infrared spectra were recorded on a Bruker FTIR Alpha Platinum ATR spectrometer. High-resolution mass spectra (HRMS) were recorded on an Agilent 6224 Accurate Mass TOF LC/MS instrument. Elemental analyses (CHN) were carried out on a Perkin-Elmer 2400 II instrument. UV/Vis spectra were collected on a Perkin-Elmer Lambda 750 UV/Vis/near-IR spectrophotometer. UV/Vis stability measurements were carried out on a Shimadzu UV-2600 UV/Vis spectrophotometer. For biological assays, 96-well plates were read using a FLUOStar Omega microplate reader. Flow cytometry analysis was conducted with a Beckman Coulter Cytoflex instrument and microscopy images were obtained with an EVOS PL system.

X-ray diffraction data were collected at 150(2) K on an Oxford Diffraction SuperNova diffractometer equipped with an Mo/Cu microfocus X-ray source ($K_\alpha$ radiation, $\lambda_{Mo} = 0.71073$ Å, $\lambda_{Cu} = 1.54184$ Å) with mirror optics and an Atlas detector. The structures were solved through the Olex$^2$ graphical user interface[46] by direct methods as implemented in SHELXT and refined by a full-matrix least-squares procedure based on $F^2$ using SHELXL.[47] All non-hydrogen atoms were refined anisotropically. Hydrogen atoms were placed in calculated positions and treated using appropriate riding models. CCDC 1912497, 1912498, 1912499, 1912500, 1912501, 1912502, 1912503, 1912504, 1912505, 1912506, 1912507, and 1912508 (**b**–**e**, **1 b**, **1 c**, **1 e**, and **2 a**–**e**) contain the supplementary crystallographic data for this paper. These data are provided free of charge by The Cambridge Crystallographic Data Centre.

**Syntheses and characterization**: Ligands **b**–**e** were prepared according to the established procedure,[21] with some modifications of N-oxidation according to another publication.[48] A general scheme for synthesis of the ligands is provided in the Supplementary Information (Figure S1). Chlorido and pta complexes were pre-

**These are not the final page numbers!** ↗↗

pared through modified versions of previously reported procedures from our group.[18,24] Physicochemical characterization of the prepared compounds was performed by $^1$H and $^{31}$P NMR spectroscopy, infrared (IR) and UV/Vis spectroscopy, CHN elemental analysis, and high-resolution electrospray ionization mass spectrometry (ESI-HRMS). Moreover, for most of the compounds, crystal structures were determined, which additionally confirmed all of the mentioned analyses. The purities of all of the synthesized compounds were confirmed through NMR spectroscopy and CHN elemental analyses. Crystal structures and $^1$H NMR and IR spectra are presented in the Supplementary Information (Figures S2–S4, S17–S34, and S35–S44, respectively).

**General procedure for obtaining b′–e′ (N-oxidation):** The requisite 2-bromomethylpyridine (1 mol. equiv.) was combined with m-chloroperoxybenzoic acid (m-CPBA, 2 mol. equiv., 70% purity) in $CH_2Cl_2$ and the mixture was stirred overnight at room temperature. The solution was first washed with 0.5 M $Na_2S_2O_{3(aq)}$ (W$_1$) and then with sat. $NaHCO_{3(aq)}$ (W$_2$). The organic phase was dried over sodium sulfate, filtered, and concentrated under reduced pressure. The residue was purified by column chromatography on silica gel, eluting with 2% MeOH/$CH_2Cl_2$. After removal of the solvent, a white solid or a light-yellow oil was obtained. Due to partitioning of N-oxides between the organic and water phases, further extractions of water phases W$_1$ and W$_2$ were needed. Water phase W$_1$ was extracted with $CH_2Cl_2$. The latter organic phase was washed with sat. $NaHCO_{3(aq)}$, which was further extracted with $CH_2Cl_2$. Water phase W$_2$ was also extracted with $CH_2Cl_2$. The combined organic layers were dried over sodium sulfate, filtered, and concentrated under reduced pressure.

**2-Bromo-3-methylpyridine-N-oxide (b′):** Yield: 72%. $^1$H NMR (500 MHz, CDCl$_3$): $\delta =8.29$–8.25 (m, 1H; Ar-$H$), 7.15–7.07 (m, 2H; Ar-$H$), 2.46 ppm (s, 3H; Ar-C$H_3$).

**2-Bromo-4-methylpyridine-N-oxide (c′):** Yield: 70%. $^1$H NMR (500 MHz, CDCl$_3$): $\delta =8.25$ (d, 1H, $J=6.6$ Hz; Ar-$H$), 7.47 (d, 1H, $J=2.1$ Hz; Ar-$H$), 7.03 (dd, 1H, $J=6.6$, 2.1 Hz; Ar-$H$), 2.33 ppm (s, 3H; Ar-C$H_3$).

**2-Bromo-5-methylpyridine-N-oxide (d′):** Yield: 75%. $^1$H NMR (500 MHz, CDCl$_3$): $\delta =8.23$ (s, 1H; Ar-$H$), 7.52 (d, 1H, $J=8.3$ Hz; Ar-$H$), 6.95–6.92 (m, 1H; Ar-$H$), 2.29 ppm (s, 3H; Ar-C$H_3$).

**2-Bromo-6-methylpyridine-N-oxide (e′):** Yield: 77%. $^1$H NMR (500 MHz, CDCl$_3$): $\delta =7.55$ (dd, 1H, $J=8.0$, 1.5 Hz; Ar-$H$), 7.23 (dd, 1H, $J=8.0$, 1.5 Hz; Ar-$H$), 7.00 (t, 1H, $J=8.0$ Hz; Ar-$H$), 2.58 ppm (s, 3H; Ar-C$H_3$).

**General procedure for obtaining b–e (thiolation):** The requisite 2-bromomethylpyridine-N-oxide b′–e′ was dissolved in a 1:1 (v/v) mixture of saturated NaSH$_{(aq)}$ and water (200 mg of substituted 2-bromopyridine-N-oxide per 20 mL of mixture) and the solution was stirred at room temperature overnight. It was then acidified to pH 1 with 4 M HCl$_{(aq)}$ and immediately extracted with CHCl$_3$. The combined organic layers were dried over sodium sulfate, filtered, and concentrated. The residue was triturated with acetone (approximately 3 mL), the by-product elemental sulfur S$_8$ was filtered off, and the mother liquor was concentrated to dryness to yield a yellow-greyish solid. Normally, the compounds thus obtained (purity > 95% based on NMR analysis) were directly used for complexation with the ruthenium precursor RuCym, as they proved to be sensitive to silica gel and partly decomposed thereon, as has been observed previously.[49] Only when ligands were needed for biological assays column chromatography on silica gel was carried out, eluting with hexane/ethyl acetate (7:3), to afford yellow-greyish solids (yields quoted below refer to before purification by column chromatography; yields after purification by column chro-

matography varied in the range 30–70%, as reported previously).[21]

**1-Hydroxy-3-methylpyridine-2(1H)-thione (b):** Yield: 80%, yellow solid. $^1$H NMR (500 MHz, CDCl$_3$): $\delta =12.47$ (br s, 1H; N-O$H$), 8.05–8.02 (m, 1H; Ar-$H$), 7.31–7.28 (m, 1H; Ar-$H$), 6.70 (t, 1H, $J=7.1$ Hz; Ar-$H$), 2.48 ppm (s, 3H; Ar-C$H_3$); ESI-HRMS (CH$_3$CN): $m/z$ calcd for $[M+H]^+$: 142.0321; found: 142.0326; elemental analysis calcd (%) for $C_6H_7NOS$: C 51.04, H 5.00, N 9.92; found: C 51.29, H 4.79, N 9.91.

**1-Hydroxy-4-methylpyridine-2(1H)-thione (c):** Yield: 91%, light-yellow solid. $^1$H NMR (500 MHz, CDCl$_3$): $\delta =12.01$ (br s, 1H; N-O$H$), 7.94 (d, 1H, $J=6.9$ Hz; Ar-$H$), 7.51 (s, 1H; Ar-$H$), 6.59 (dd, 1H, $J=6.9$, 2.2 Hz; Ar-$H$), 2.28 ppm (s, 3H; Ar-C$H_3$); ESI-HRMS (CH$_3$CN): $m/z$ calcd for $[M+H]^+$: 142.0321; found: 142.0321; elemental analysis calcd (%) for $C_6H_7NOS$: C 51.04, H 5.00, N 9.92; found: C 51.01, H 4.66, N 9.85.

**1-Hydroxy-5-methylpyridine-2(1H)-thione (d):** Yield: 85%, light-yellow solid. $^1$H NMR (500 MHz, CDCl$_3$): $\delta =12.10$ (br s, 1H; N-O$H$), 7.91 (s, 1H; Ar-$H$), 7.59 (d, 1H, $J=8.7$ Hz; Ar-$H$), 7.13 (dd, 1H, $J=8.7$, 1.7 Hz; Ar-$H$), 2.26 ppm (s, 3H; Ar-C$H_3$); ESI-HRMS (CH$_3$CN): $m/z$ calcd for $[M+H]^+$: 142.0321; found: 142.0323; elemental analysis calcd (%) for $C_6H_7NOS$: C 51.04, H 5.00, N 9.92; found: C 51.24, H 4.86, N 10.23.

**1-Hydroxy-6-methylpyridine-2(1H)-thione (e):** Yield: 85%, greyish solid. $^1$H NMR (500 MHz, CDCl$_3$): $\delta =12.59$ (br s, 1H; N-O$H$), 7.56 (dd, 1H, $J=8.4$, 1.0 Hz; Ar-$H$), 7.17 (dd, 1H, $J=8.4$, 7.5 Hz; Ar-$H$), 6.61 (dd, 1H, $J=7.5$, 1.0 Hz; Ar-$H$), 2.58 ppm (s, 3H; Ar-C$H_3$); ESI-HRMS (CH$_3$CN): $m/z$ calcd for $[M+H]^+$: 142.0321; found: 142.0326; elemental analysis calcd (%) for $C_6H_7NOS$: C 51.04, H 5.00, N 9.92; found: C 50.93, H 5.01, N 9.68.

**General procedure for obtaining 1a–e:** A reaction mixture containing the appropriate ligand a–e (90 mg, 2 mol. equiv.), precursor RuCym (1 mol. equiv.), and NaOMe (1.9 mol. equiv.) as base in acetone was stirred overnight at room temperature. The solvent was then removed under reduced pressure using a rotary evaporator, and the crude product was purified by column chromatography on silica gel, eluting with 5% CH$_2$Cl$_2$/acetone. After combining the appropriate fractions, the mobile phase was evaporated under reduced pressure to leave an oily residue. To ensure complete removal of the methanol, the residue was redissolved in CH$_2$Cl$_2$ (ca. 10 mL) and the solvent was again evaporated. The oily product was redissolved in CH$_2$Cl$_2$ (1–2 mL), and the addition of cold n-heptane (10–15 mL) usually resulted in precipitation of the complex. Otherwise, the solvents were partly evaporated using a rotary evaporator, whereupon a red solid precipitated. An ultrasonic bath was also sometimes used to aid precipitation. The suspension was left to stand for 15 min, and then the product was collected by filtration under reduced pressure and washed with cold n-heptane. The obtained red solids was left to dry overnight at 45 °C.

**[(η$^6$-p-Cymene)Ru(1-hydroxypyridine-2(1H)-thionato)Cl] (1a):** Yield: 57% (160 mg), red solid. $^1$H NMR (500 MHz, CDCl$_3$): $\delta =8.03$ (dd, 1H, $J=6.8$, 0.8 Hz; Ar-$H$ a), 7.44 (dd, 1H, $J=8.3$, 1.3 Hz; Ar-$H$ a), 7.05–7.00 (m, 1H; Ar-$H$ a), 6.71 (td, 1H, $J=6.8$, 1.6 Hz; Ar-$H$ a), 5.47 (d, 2H, $J=6.0$ Hz; Ar-$H$ cym), 5.27 (d, 2H, $J=6.0$ Hz; Ar-$H$ cym), 2.82 (hept, 1H, $J=6.9$ Hz; Ar-C$H$(CH$_3$)$_2$ cym), 2.24 (s, 3H; Ar-C$H_3$ cym), 1.27 ppm (d, 6H, $J=6.9$ Hz; Ar-CH(C$H_3$)$_2$ cym); IR selected bands (ATR): $\tilde{v} =3034$, 2964, 2870, 1544, 1453, 1172, 1131, 765, 708, 622 cm$^{-1}$; UV/Vis ($\lambda$ ($\varepsilon$), $c=5\times10^{-5}$ M, MeOH): 284 (10268), 490 nm (488 Lmol$^{-1}$cm$^{-1}$); ESI-HRMS (CH$_3$CN): $m/z$ calcd for $[M-Cl]^+$: 362.0153; found: 362.0149; elemental analysis calcd (%) for $C_{15}H_{18}ClNORuS$: C 45.39, H 4.57, N 3.53; found: C 45.13, H 4.29, N 3.50.

**↖↖ These are not the final page numbers!**

**[(η⁶-*p*-Cymene)Ru(1-hydroxy-3-methylpyridine-2(1*H*)-thionato)Cl] (1 b)**: Yield: 52 % (135 mg), red solid. ¹H NMR (500 MHz, CDCl₃): $\delta =$ 7.97 (dd, 1 H, $J = 6.8$, 0.6 Hz; Ar-*H* b), 6.97 (dt, 1 H, $J = 7.1$, 1.0 Hz; Ar-*H* b), 6.66 (t, 1 H, $J = 7.1$ Hz; Ar-*H* b), 5.48 (d, 2 H, $J = 6.0$ Hz; Ar-*H* cym), 5.27 (d, 2 H, $J = 6.0$ Hz; Ar-*H* cym), 2.82 (hept, 1 H, $J = 7.0$ Hz; Ar-C*H*(CH₃)₂ cym), 2.41 (s, 3 H; Ar-C*H₃* b), 2.24 (s, 3 H; Ar-C*H₃* cym), 1.26 ppm (d, 6 H, $J = 7.0$ Hz; Ar-CH(C*H₃*)₂ cym); IR selected bands (ATR): $\tilde{\nu} =$ 3102, 2961, 2861, 1558, 1402, 1193, 1136, 1072, 777, 657 cm⁻¹; UV/Vis ($\lambda$ ($\varepsilon$), $c = 5 \times 10^{-5}$ M, MeOH): 276 (12260), 488 nm (568 L mol⁻¹ cm⁻¹); ESI-HRMS (CH₃CN): *m/z* calcd for [*M*−Cl]⁺: 376.0309; found: 376.0315; elemental analysis calcd (%) for C₁₆H₂₀ClNORuS: C 46.77, H 4.91, N 3.41; found: C 46.45, H 4.86, N 3.30.

**[(η⁶-*p*-Cymene)Ru(1-hydroxy-4-methylpyridine-2(1*H*)-thionato)Cl] (1 c)**: Yield: 57 % (150 mg), red solid. ¹H NMR (500 MHz, CDCl₃): $\delta =$ 7.90 (d, 1 H, $J = 6.9$ Hz; Ar-*H* c), 7.23 (d, 1 H, $J = 1.3$ Hz; Ar-*H* c), 6.51 (dd, 1 H, $J = 6.9$, 1.9 Hz; Ar-*H* c), 5.45 (d, 2 H, $J = 5.9$ Hz; Ar-*H* cym), 5.25 (d, 2 H, $J = 5.9$ Hz; Ar-*H* cym), 2.82 (hept, 1 H, $J = 7.0$ Hz; Ar-C*H*(CH₃)₂ cym), 2.24 (s, 3 H; Ar-C*H₃* cym), 2.17 (s, 3 H; Ar-C*H₃* c), 1.27 ppm (d, 6 H, $J = 7.0$ Hz; Ar-CH(C*H₃*)₂ cym); IR selected bands (ATR): $\tilde{\nu} =$ 3097, 2959, 2865, 1464, 1167, 1131, 856, 800, 775, 621 cm⁻¹; UV/Vis ($\lambda$ ($\varepsilon$), $c = 5 \times 10^{-5}$ M, MeOH): 283 (12962), 489 nm (574 L mol⁻¹ cm⁻¹); ESI-HRMS (CH₃CN): *m/z* calcd for [*M*−Cl]⁺: 376.0309; found: 376.0317; elemental analysis calcd (%) for C₁₆H₂₀ClNORuS: C 46.77, H 4.91, N 3.41; found: C 46.73, H 4.92, N 3.45.

**[(η⁶-*p*-Cymene)Ru(1-hydroxy-5-methylpyridine-2(1*H*)-thionato)Cl] (1 d)**: Yield: 52 % (137 mg), red solid. ¹H NMR (500 MHz, CDCl₃): $\delta =$ 7.89 (s, 1 H; Ar-*H* d), 7.32 (d, 1 H, $J = 8.4$ Hz; Ar-*H* d), 6.87 (dd, 1 H, $J = 8.4$, 1.1 Hz; Ar-*H* d), 5.46 (d, 2 H, $J = 6.1$ Hz; Ar-*H* cym), 5.25 (d, 2 H, $J = 6.1$ Hz; Ar-*H* cym), 2.82 (hept, 1 H, $J = 6.9$ Hz; Ar-C*H*(CH₃)₂ cym), 2.24 (s, 3 H; Ar-C*H₃* cym), 2.14 (s, 3 H; Ar-C*H₃* d), 1.27 ppm (d, 6 H, $J = 6.9$ Hz; Ar-CH-(C*H₃*)₂ cym); IR selected bands (ATR): $\tilde{\nu} =$ 3041, 2959, 2865, 1477, 1145, 850, 814, 744, 671, 542 cm⁻¹; UV/Vis ($\lambda$ ($\varepsilon$), $c = 5 \times 10^{-5}$ M, MeOH): 281 (11358), 489 nm (518 L mol⁻¹ cm⁻¹); ESI-HRMS (CH₃CN): *m/z* calcd for [*M*−Cl]⁺: 376.0309; found: 376.0315; elemental analysis calcd (%) for C₁₆H₂₀ClNORuS: C 46.77, H 4.91, N 3.41; found: C 46.78, H 4.81, N 3.37.

**[(η⁶-*p*-Cymene)Ru(1-hydroxy-6-methylpyridine-2(1*H*)-thionato)Cl] (1 e)**: Yield: 57 % (149 mg), red solid. ¹H NMR (500 MHz, CDCl₃): $\delta =$ 7.31 (d, 1 H, $J = 8.1$ Hz; Ar-*H* e), 6.91 (t, 1 H, $J = 7.6$ Hz; Ar-*H* e), 6.61 (dd, 1 H, $J = 7.3$, 0.7 Hz; Ar-*H* e), 5.50 (d, 2 H, $J = 4.4$ Hz; Ar-*H* cym), 5.23 (s, 2 H; Ar-*H* cym), 2.83 (hept, 1 H, $J = 7.0$ Hz; Ar-C*H*(CH₃)₂ cym), 2.50 (s, 3 H; Ar-C*H₃* e), 2.24 (s, 3 H; Ar-C*H₃* cym), 1.31 ppm (d, 6 H, $J = 7.0$ Hz; Ar-CH(C*H₃*)₂ cym); IR selected bands (ATR): $\tilde{\nu} =$ 3036, 2956, 2867, 1552, 1458, 1197, 1155, 863, 776, 651 cm⁻¹; UV/Vis ($\lambda$ ($\varepsilon$), $c = 5 \times 10^{-5}$ M, MeOH): 279 (9832), 483 nm (510 L mol⁻¹ cm⁻¹); ESI-HRMS (CH₃CN): *m/z* calcd for [*M*−Cl]⁺: 376.0309; found: 376.0310; elemental analysis calcd (%) for C₁₆H₂₀ClNORuS: C 46.77, H 4.91, N 3.41; found: C 46.58, H 4.79, N 3.40.

**General procedure for obtaining 2 a–e**: A reaction mixture containing the appropriate chlorido complex **1 a–e** (80 mg, 1 mol. equiv.), ground phosphine ligand pta (1.5 mol. equiv.), and NH₄PF₆ (1.5 mol. equiv.) in dichloromethane (30 mL) was stirred in the dark at room temperature for 48 h, during which the colour changed from red-orange to orange. The mixture was concentrated using a rotary evaporator and the resulting suspension was filtered through a Celite pad to remove precipitated NH₄Cl, unreacted NH₄PF₆, and pta. The mother liquor was concentrated (to approximately 2 mL) to obtain an oily residue. Addition of cold diethyl ether (10–20 mL) resulted in precipitation of the product. If needed, an ultrasonic bath was used to aid precipitation. The suspension was left to stand for 10 min at 4 °C, and then the product was collected by filtration and washed with diethyl ether. The yellow-orange solids was left to dry at 45 °C overnight.

**[(η⁶-*p*-Cymene)Ru(1-hydroxypyridine-2(1*H*)-thionato)pta]PF₆ (2 a)**: Yield: 74 % (99 mg), light-yellow solid. ¹H NMR (500 MHz, (CD₃)₂CO)): $\delta =$ 8.31 (dd, 1 H, $J = 6.9$, 0.6 Hz; Ar-*H* a), 7.67 (dd, 1 H, $J = 8.3$, 1.2 Hz; Ar-*H* a), 7.47–7.41 (m, 1 H; Ar-*H* a), 7.14 (td, 1 H, $J = 6.9$, 1.7 Hz; Ar-*H* a), 6.29 (d, 1 H, $J = 6.1$ Hz; Ar-*H* cym), 6.19 (d, 1 H, $J = 6.1$ Hz; Ar-*H* cym), 6.03 (d, 1 H, $J = 6.1$ Hz; Ar-*H* cym), 5.87 (d, 1 H, $J = 6.1$ Hz; Ar-*H* cym), 4.50 (s, 6 H; *H* pta), 4.28–4.11 (m, 6 H; *H* pta), 2.71 (hept, 1 H, $J = 7.0$ Hz; Ar-C*H*(CH₃)₂ cym), 2.15 (s, 3 H; Ar-C*H₃* cym), 1.26 ppm (dd, 6 H, $J = 15.2$, 7.0 Hz; Ar-CH(C*H₃*)₂ cym); ³¹P NMR (202 MHz, (CD₃)₂CO)): $\delta = -31.62$ (*P*-pta), −144.25 ppm (hept, $J_{PF} = 708$ Hz; *PF₆*); IR selected bands (ATR): $\tilde{\nu} =$ 3112, 2932, 1460, 1242, 974, 947, 834, 765, 557, 481 cm⁻¹; UV/Vis ($\lambda$ ($\varepsilon$), $c = 5 \times 10^{-5}$ M, MeOH): 297 (10986), 375 nm (2150 L mol⁻¹ cm⁻¹); ESI-HRMS (CH₃CN): *m/z* calcd for [*M*−PF₆]⁺: 519.0921; found: 519.0924; elemental analysis calcd (%) for C₂₁H₃₀F₆N₄OP₂RuS: C 38.01, H 4.56, N 8.44; found: C 37.89, H 4.43, N 8.29.

**[(η⁶-*p*-Cymene)Ru(1-hydroxy-3-methylpyridine-2(1*H*)-thionato)-pta]PF₆ (2 b)**: Yield: 83 % (110 mg), light-yellow solid. ¹H NMR (500 MHz, (CD₃)₂CO)): $\delta =$ 8.20 (d, 1 H, $J = 6.7$ Hz; Ar-*H* b), 7.39 (d, 1 H, $J = 7.1$ Hz; Ar-*H* b), 7.07 (t, 1 H, $J = 7.1$ Hz; Ar-*H* b), 6.28 (d, 1 H, $J = 6.1$ Hz; Ar-*H* cym), 6.18 (d, 1 H, $J = 6.1$ Hz; Ar-*H* cym), 6.03 (d, 1 H, $J = 6.1$ Hz; Ar-*H* cym), 5.86 (d, 1 H, $J = 6.1$ Hz; Ar-*H* cym), 4.48 (s, 6 H; *H* pta), 4.26–4.08 (m, 6 H; *H* pta), 2.73 (hept, 1 H, $J = 6.9$ Hz; Ar-C*H*(CH₃)₂ cym), 2.48 (s, 3 H; Ar-C*H₃* b), 2.17 (s, 3 H; Ar-C*H₃* cym), 1.27 ppm (dd, 6 H, $J = 16.2$, 6.9 Hz; Ar-CH(C*H₃*)₂ cym); ³¹P NMR (202 MHz, (CD₃)₂CO)): $\delta = -31.70$ (*P*-pta), −144.25 ppm (hept, $J_{PF} = 707$ Hz; *PF₆*); IR selected bands (ATR): $\tilde{\nu} =$ 3087, 2964, 2875, 1427, 1240, 972, 946, 829, 581, 556 cm⁻¹; UV/Vis ($\lambda$ ($\varepsilon$), $c = 5 \times 10^{-5}$ M, MeOH): 290 (12238), 369 nm (2782 L mol⁻¹ cm⁻¹); ESI-HRMS (CH₃CN): *m/z* calcd for [*M*−PF₆]⁺: 533.1078; found: 533.1078; elemental analysis calcd (%) for C₂₂H₃₂F₆N₄OP₂RuS: C 39.00, H 4.76, N 8.27; found: C 39.02, H 4.72, N 7.99.

**[(η⁶-*p*-Cymene)Ru(1-hydroxy-4-methylpyridine-2(1*H*)-thionato)-pta]PF₆ (2 c)**: Yield: 80 % (106 mg), dark-orange solid. ¹H NMR (500 MHz, (CD₃)₂CO)): $\delta =$ 8.16 (d, 1 H, $J = 6.9$ Hz; Ar-*H* c), 7.48 (s, 1 H; Ar-*H* c), 6.97 (dd, 1 H, $J = 6.9$, 2.1 Hz; Ar-*H* c), 6.26 (d, 1 H, $J = 6.1$ Hz; Ar-*H* cym), 6.16 (d, 1 H, $J = 6.1$ Hz; Ar-*H* cym), 6.01 (d, 1 H, $J = 6.1$ Hz; Ar-*H* cym), 5.85 (d, 1 H, $J = 6.1$ Hz; Ar-*H* cym), 4.50 (s, 6 H; *H* pta), 4.26–4.10 (m, 6 H; *H* pta), 2.69 (hept, 1 H, $J = 6.9$ Hz; Ar-C*H*(CH₃)₂ cym), 2.30 (s, 3 H; Ar-C*H₃* c), 2.14 (s, 3 H; Ar-C*H₃* cym), 1.25 ppm (dd, 6 H, $J = 14.3$, 6.9 Hz; Ar-CH(C*H₃*)₂ cym); ³¹P NMR (202 MHz, (CD₃)₂CO)): $\delta = -31.58$ (*P*-pta), −147.74 ppm (hept, $J_{PF} = 708$ Hz; *PF₆*); IR selected bands (ATR): $\tilde{\nu} =$ 2967, 2881, 1467, 1245, 974, 947, 832, 742, 581, 556 cm⁻¹; UV/Vis ($\lambda$ ($\varepsilon$), $c = 5 \times 10^{-5}$ M, MeOH): 296 (11644), 379 nm (2062 L mol⁻¹ cm⁻¹); ESI-HRMS (CH₃CN) *m/z* calcd for [*M*−PF₆]⁺: 533.1078; found: 533.1075; elemental analysis calcd (%) for C₂₂H₃₂F₆N₄OP₂RuS: C 39.00, H 4.76, N 8.27; found: C 38.92, H 4.74, N 8.06.

**[(η⁶-*p*-Cymene)Ru(1-hydroxy-5-methylpyridine-2(1*H*)-thionato)-pta]PF₆ (2 d)**: Yield: 79 % (105 mg), light-yellow solid. ¹H NMR (500 MHz, (CD₃)₂CO)): $\delta =$ 8.18 (s, 1 H; Ar-*H* d), 7.55 (d, 1 H, $J = 8.3$ Hz; Ar-*H* d), 7.33–7.29 (m, 1 H; Ar-*H* d), 6.27 (d, 1 H, $J = 6.1$ Hz; Ar-*H* cym), 6.17 (d, 1 H, $J = 6.1$ Hz; Ar-*H* cym), 6.02 (d, 1 H, $J = 6.1$ Hz; Ar-*H* cym), 5.84 (d, 1 H, $J = 6.1$ Hz; Ar-*H* cym), 4.50 (s, 6 H; *H* pta), 4.27–4.09 (m, 6 H; *H* pta), 2.70 (hept, 1 H, $J = 7.0$ Hz; Ar-C*H*(CH₃)₂ cym), 2.27 (s, 3 H; Ar-C*H₃* d), 2.14 (s, 3 H; Ar-C*H₃* cym), 1.25 ppm (dd, 6 H, $J = 13.7$, 7.0 Hz; Ar-CH(C*H₃*)₂ cym); ³¹P NMR (202 MHz, (CD₃)₂CO)): $\delta = -31.67$ (*P*-pta), −144.25 ppm (hept, $J_{PF} = 708$ Hz; *PF₆*); IR selected bands (ATR): $\tilde{\nu} =$ 2964, 2878, 1479, 1141, 972, 946, 833, 740, 576, 566 cm⁻¹; UV/Vis ($\lambda$ ($\varepsilon$), $c = 5 \times 10^{-5}$ M, MeOH): 296 (11754), 379 nm (2192 L mol⁻¹ cm⁻¹); ESI-HRMS (CH₃CN): *m/z* calcd

These are not the final page numbers! ↗↗

for $[M-PF_6]^+$: 533.1078; found: 533.1080; elemental analysis calcd (%) for $C_{22}H_{32}F_6N_4OP_2RuS$: C 39.00, H 4.76, N 8.27; found: C 38.89, H 4.76, N 8.09.

**[($\eta^6$-*p*-Cymene)Ru(1-hydroxy-6-methylpyridine-2(1*H*)-thionato)p-ta]PF$_6$ (2e):** Yield: 85% (112 mg), light-orange solid. $^1$H NMR (500 MHz, (CD$_3$)$_2$CO)): $\delta = 7.53$ (dd, 1H, $J = 8.3$, 1.0 Hz; Ar-*H* e), 7.32 (t, 1H, $J = 7.3$ Hz; Ar-*H* e), 7.06 (dd, 1H, $J = 7.3$, 1.0 Hz; Ar-*H* e), 6.31 (d, 1H, $J = 6.1$ Hz; Ar-*H* cym), 6.22 (d, 1H, $J = 6.1$ Hz; Ar-*H* cym), 6.03 (d, 1H, $J = 6.1$ Hz; Ar-*H* cym), 5.85 (d, 1H, $J = 6.1$ Hz; Ar-*H* cym), 4.54–4.45 (m, 6H; *H* pta), 4.28–4.09 (m, 6H; *H* pta), 2.74 (hept, 1H, $J = 6.9$ Hz; Ar-C*H*(CH$_3$)$_2$ cym), 2.53 (s, 3H; Ar-C*H$_3$* e), 2.17 (s, 3H; Ar-C*H$_3$* cym), 1.29 ppm (dd, 6H, $J = 19.2$, 6.9 Hz; Ar-CH(C*H$_3$*)$_2$ cym); $^{31}$P NMR (202 MHz, (CD$_3$)$_2$CO)): $\delta = -31.28$ (*P*-pta), $-144.25$ ppm (hept, $J_{PF} = 707$ Hz; *P*F$_6$); IR selected bands (ATR): $\tilde{\nu} = 3096$, 2966, 2878, 1461, 1014, 974, 947, 834, 581, 557 cm$^{-1}$; UV/Vis ($\lambda$ ($\varepsilon$), $c = 5 \times 10^{-5}$ M, MeOH): 289 (8670), 364 nm (2424 L mol$^{-1}$ cm$^{-1}$); ESI-HRMS (CH$_3$CN): *m/z* calcd for $[M-PF_6]^+$: 533.1078; found: 533.1075; elemental analysis calcd (%) for $C_{22}H_{32}F_6N_4OP_2RuS$: C 39.00, H 4.76, N 8.27; found: C 38.96, H 4.69, N 8.27.

**UV/Vis stability:** Stability over 24 h was assessed in biologically relevant matrixes, namely a) water, b) PBS, c) RPMI-1640, d) fully prepared RPMI-1640 to which 10% (v/v) fetal calf serum and 1% (v/v) penicillin/streptomycin antibiotics had been added, and e) human blood plasma. For these experiments, stock solutions of all complexes were prepared in DMSO and further diluted with the corresponding matrices. UV/Vis spectra were obtained twice (0 h and 24 h) over the range 250–900 nm through single-beam scans with background correction. Samples were kept in sealed cuvettes at 37 °C between measurements.

**Cell culture:** All cell lines were obtained from the European Collection of Cell Cultures (ECACC). They were grown in Roswell Park Memorial Institute medium (RPMI-1640) supplemented with 10% fetal calf serum, 1% (v/v) 2 mM glutamine, and 1% (v/v) penicillin/streptomycin (equivalent to 100 units mL$^{-1}$). Cells were grown as adherent monolayers in 25 or 75 cm$^2$ culture flasks at 37 °C in a 5% CO$_2$ humidified atmosphere and passaged at regular intervals, once 80% confluence was reached, using trypsin-EDTA.

**Cytotoxicity assays: determination of IC$_{50}$ values:** Briefly, 5000 cells were seeded per well in flat-bottomed 96-well plates. The cells were pre-incubated in drug-free media at 37 °C for 48 h before adding different concentrations of the compounds to be tested. A stock solution of the compound was firstly prepared in 5% v/v DMSO and a mixture 0.9% saline and cell culture medium (1:1) (v/v) following serial dilutions in RPMI-1640 to achieve working solutions in which DMSO concentration did not exceed 0.5% v/v. The drug exposure period was 24 h. Thereafter, supernatants were removed by suction and each well was washed with PBS. A further 72 h was allowed for the cells to recover in drug-free medium at 37 °C. MTT assay was used to determine cell viability, with 4 h dye exposure in the dark. Absorbance measurements of the solubilized dye in DMSO allowed the determination of viable treated cells compared to untreated controls. IC$_{50}$ values (concentrations causing 50% cell growth inhibition) were determined as duplicates of triplicates in two independent sets of experiments and their standard deviations were calculated.

**Wound healing assay:** A549 lung cancer cells were seeded in 24-well plates at 10000 cells/well and allowed to reach 90% confluence. Following attachment, two "wounds" were created in each well using a pipette tip and cells were treated with complexes **1b** and **2b** using solutions as described above. After 24 h of drug exposure, the drugs were removed by suction, and the cells were washed with PBS and stained with crystal violet solution prepared with 10% ethanol. Excess staining agent was removed by washing

with PBS, and cells were visualized using a 4× transmission microscope. A graph and numerical data can be found in the Supplementary Information (Figure S13 and Table S4).

**Induction of apoptosis:** The induction of cell death mechanism was investigated by means of flow cytometry and fluorescence microscopy using Annexin V-FITC and PI. For the former, A549 lung cancer cells were seeded in six-well plates and allowed to attach for 24 h. Following attachment, cells were treated with complexes **1b** and **2b** using solutions as described above. After a drug exposure time of 24 h, the drugs were removed by suction and the cells were washed with PBS and detached using trypsin. Individual cell suspensions were stained using PI/Annexin V-FITC in buffer. This experiment included negative untreated controls, and positive control cells induced with staurosporine (1 µg mL$^{-1}$). Cells for apoptosis studies were used with no previous fixing procedure so as to avoid non-specific binding of the Annexin V-FITC conjugate. These experiments were carried out in triplicate, and full numerical data and statistical analysis can be found in the Supplementary Information (Table S5). For fluorescence microscopy experiments, cells were seeded in eight-well microscopy chambers at 5000 cells/well. Drug treatment and staining were carried out as described above and readings were obtained using an EVOS FL microscope.

**Cell cycle analysis:** A million A549 lung carcinoma cells were seeded in six-well plates. Cells were allowed to attach for 24 h in a 5% CO$_2$ incubator before adding various concentrations of complexes **1b** and **2b**. Drug solutions were prepared similarly to those used in the cytotoxicity assays, such that the DMSO concentration did not exceed 1%. Following 24 h of drug exposure, the drugs were removed by suction, and the cells were washed with PBS and detached using trypsin-EDTA. Individual cell solutions were obtained and centrifuged to produce cell pellets, which were fixed for 2 h using ice-cold ethanol. Following fixation, cell pellets were stained by re-suspending them in PBS containing PI and RNAse A. Samples were analysed by flow cytometry with excitation of the PI-bound DNA maximum at 536 nm, eliciting its emission at 617 nm. Data were processed using Flowjo software. In these experiments, untreated cells served as negative controls. The experiments were carried out in triplicate, and full numerical data and statistical analysis can be found in the Supplementary Information (Table S6).

**CT-DNA UV/Vis interactions:** UV/Vis spectrophotometric investigations were performed to determine the DNA-binding affinities of complexes **1b** and **2b**. Experiments were carried out by keeping the concentration of CT-DNA fixed (75 µM) while varying the concentrations of the metal complexes (0, 5, 25, 50, 75, 100, 150, and 200 µM). Absorbance spectra were recorded at 10 min after mixing the solutions and again 24 h later. Graphs can be found in the Supplementary Information (Figures S15 and S16).

**CT-DNA melting:** CT-DNA experiments were carried out in 10 mM phosphate buffer containing 100 mM NaCl at pH 7.5. In order to confirm that the CT-DNA was free from proteins, its UV/Vis spectrum was measured in phosphate buffer, giving an absorbance ratio of 1.92:1 at 260 nm/280 nm. Its concentration was determined based on the UV absorbance at 260 nm and the known extinction coefficient at this wavelength (6600 dm$^3$ mol$^{-1}$ cm$^{-1}$). Thermal denaturation of CT-DNA was recorded by measuring its absorbance at 260 nm upon increasing the temperature from 50 °C to 95 °C. The melting curves of single CT-DNA or CT-DNA/complexes were recorded at a fixed ratio of 1:1 CT-DNA/complex (75 µM). The melting temperature (T$_m$), at which 50% of the double-stranded CT-DNA present is converted into single-stranded CT-DNA, was determined as the corresponding maximum on the

**↖↖ These are not the final page numbers!**

first-derivative profile of the melting curve. Numerical data can be found in the Supplementary Information (Table S7).

**Induction of reactive oxygen species (ROS)**: A549 lung carcinoma cells were seeded in black 96-well plates at 10000 cells per well. Cells were allowed to attach for 24 h before adding increasing concentrations of complexes **1 b** and **2 b**. The working solutions used were obtained as described for the cytotoxicity assays. After drug exposure for 24 h, supernatants were removed by suction and the plates were washed with PBS. An aliquot (100 μL) of a 50 μM solution of 2′,7′-dichlorofluorescein diacetate (DCFH-DA) was added to each well, and the plates were incubated with the dye in the dark for 2 h at 37 °C. Once the cells were stained, the supernatants were removed by suction and the wells were washed with PBS before adding ROS inducers as positive controls. Hydrogen peroxide was used at 1 mM and *tert*-butyl hydroperoxide (TBHP) at 500 μM. ROS induction by positive controls was allowed to proceed for 2 h in the dark at 37 °C. Fluorescence readings were obtained by excitation at 485 nm, giving rise to emission at 530 nm. This experiment included negative untreated controls, controls only treated with the metal complexes (to discard autofluorescence), untreated cells with hydrogen peroxide or TBHP, and complex-treated cells with the ROS inducers.

**Evaluation of mitochondrial function**: A549 lung cancer cells were seeded in eight-well microscopy chambers at 5000 cells/well and allowed to attach for 24 h. Following attachment, the cells were treated with solutions of complexes **1 b** and **2 b** prepared as described above. After a drug exposure time of 24 h, the drugs were removed by suction, and the cells were washed with PBS and stained using DAPI/PI/Rh-123 in buffer. Readings were taken using an EVOS FL microscope. In these experiments, untreated cells served as negative controls.

**Statistical analysis**: In all cases, independent two-sample t-tests with unequal variances, Welch's tests, were carried out to establish the statistical significance of the variations ($p < 0.01$ for **, and $p < 0.05$ for *).

**Binding to albumin and inhibton of TrxR**: The experiments were performed as described in our previous reports.[40,42,50]

## Supplementary Information

General scheme for synthesis of the ligands (Figure S1); crystallographic data and structures for **b**–**e**, **1 b**–**c**, **1 e**, and **2 a**–**e** (Tables S1–S3 and Figures S2–S4); aqueous stability of **1 b** and **2 b** followed by UV/Vis spectroscopy (Figures S5 and S6); aqueous stability of **1 b** and **2 b** followed by $^{1}$H and $^{31}$P NMR spectroscopy (Figures S7–S12); graph and numerical data for wound healing assay (Figure S13, Table S4); control data for induction of apoptosis in A549 cells (Table S5); optical microscopy observations of A549 cells (Figure S14); control data for cell cycle analysis in A549 cells (Table S6); values of CT-DNA melting assays (Table S7); UV/Vis spectral titrations of CT-DNA with complexes **1 b** and **2 b** (Figures S15 and S16); $^{1}$H NMR spectra of **b′**–**e′**, **b**–**e**, **1 a**–**e**, and **2 a**–**e** (Figures S17–S34); IR spectra of **1 a**–**e** and **2 a**–**e** (Figures S35–S44).

## Acknowledgements

## Conflict of interest

The authors declare no conflict of interest.

[1] B. Rosenberg, L. Vancamp, J. E. Trosko, V. H. Mansour, *Nature* **1969**, *222*, 385–386.

[2] a) L. Kelland, *Nat. Rev. Cancer* **2007**, *7*, 573–584; b) I. Romero-Canelón, P. J. Sadler, *Proc. Natl. Acad. Sci. USA* **2015**, *112*, 4187–4188.

[3] a) H. A. Burris, S. Bakewell, J. C. Bendell, J. Infante, S. F. Jones, D. R. Spigel, G. J. Weiss, R. K. Ramanathan, A. Ogden, D. Von Hoff, *Esmo Open* **2016**, *1*, DOI: 10.1136/esmoopen-2016-000154; b) S. Thota, D. A. Rodrigues, D. C. Crans, E. J. Barreiro, *J. Med. Chem.* **2018**, *61*, 5805–5821; c) S. Monro, K. L. Colón, H. Yin, J. Roque, P. Konda, S. Gujar, R. P. Thummel, L. Lilge, C. G. Cameron, S. A. McFarland, *Chem. Rev.* **2019**, *119*, 797–828.

[4] a) C. Scolaro, A. Bergamo, L. Brescacin, R. Delfino, M. Cocchietto, G. Laurenczy, T. J. Geldbach, G. Sava, P. J. Dyson, *J. Med. Chem.* **2005**, *48*, 4161–4171; b) P. Nowak-Sliwinska, J. R. van Beijnum, A. Casini, A. A. Nazarov, G. Wagnieres, H. van den Bergh, P. J. Dyson, A. W. Griffioen, *J. Med. Chem.* **2011**, *54*, 3895–3902.

[5] L. Zeng, P. Gupta, Y. Chen, E. Wang, L. Ji, H. Chao, Z. S. Chen, *Chem. Soc. Rev.* **2017**, *46*, 5771–5804.

[6] a) G. Süss-Fink, *Dalton Trans.* **2010**, *39*, 1673–1688; J. Kljun, I. Turel, *Eur. J. Inorg. Chem.* **2017**, 1655–1666; b) J. Kljun, I. E. Leon, S. Peršič, J. F. Cadavid-Vargas, S. B. Etcheverry, W. He, Y. Bai, I. Turel, *J. Inorg. Biochem.* **2018**, *186*, 187–196.

[7] a) R. Hudej, J. Kljun, W. Kandioller, U. Repnik, B. Turk, C. G. Hartinger, B. K. Keppler, D. Miklavcic, I. Turel, *Organometallics* **2012**, *31*, 5867–5874; b) M. Schmidlehner, L. S. Flocke, A. Roller, M. Hejl, M. A. Jakupec, W. Kandioller, B. K. Keppler, *Dalton Trans.* **2016**, *45*, 724–733; c) W. Kandioller, C. G. Hartinger, A. A. Nazarov, M. L. Kuznetsov, R. O. John, C. Bartel, M. A. Jakupec, V. B. Arion, B. K. Keppler, *Organometallics* **2009**, *28*, 4249–4251.

[8] E. Shaw, J. Bernstein, K. Losee, W. A. Lott, *J. Am. Chem. Soc.* **1950**, *72*, 4362–4364.

[9] R. A. Jones, A. R. Katritzky, *J. Chem. Soc.* **1960**, *0*, 2937–2942.

[10] A. Bond, W. Jones, *Acta Crystallogr. Sect. C* **1999**, *55*, 1536–1538.

[11] N. L. Reeder, J. Kaplan, J. Xu, R. S. Youngquist, J. Wallace, P. Hu, K. D. Juhlin, J. R. Schwartz, R. A. Grant, A. Fieno, S. Nemeth, T. Reichling, J. P. Tiesman, T. Mills, M. Steinke, S. L. Wang, C. W. Saunders, *Antimicrob. Agents Chemother.* **2011**, *55*, 5753–5760.

[12] I. Machado, L. B. Marino, B. Demoro, G. A. Echeverria, O. E. Piro, C. Q. F. Leite, F. R. Pavan, D. Gambino, *Eur. J. Med. Chem.* **2014**, *87*, 267–273.

[13] E. Rodríguez Arce, M. F. Mosquillo, L. Perez-Diaz, G. A. Echeverria, O. E. Piro, A. Merlino, E. L. Coitiño, C. Maringolo Ribeiro, C. Q. F. Leite, F. R. Pavan, L. Otero, D. Gambino, *Dalton Trans.* **2015**, *44*, 14453–14464.

[14] a) H. Sakurai, H. Sano, T. Takino, H. Yasui, *Chem. Lett.* **1999**, *28*, 913–914; b) S. Takeshita, I. Kawamura, T. Yasuno, C. Kimura, T. Yamamoto, J. Seki, A. Tamura, H. Sakurai, T. Goto, *J. Inorg. Biochem.* **2001**, *85*, 179–186.

[15] C. Zhao, X. Chen, D. Zang, X. Lan, S. Liao, C. Yang, P. Zhang, J. Wu, X. Li, N. Liu, Y. Liao, H. Huang, X. Shi, L. Jiang, X. Liu, Z. He, Q. P. Dou, X. Wang, J. Liu, *Oncogene* **2016**, *35*, 5916–5927.

[16] C. Ma, J. Zhang, R. Zhang, *Can. J. Chem.* **2003**, *81*, 1070–1075.

[17] I. R. Baird, R. Mosi, M. Olsen, B. R. Cameron, S. P. Fricker, R. T. Skerlj, *Inorg. Chim. Acta* **2006**, *359*, 2736–2750.

[18] J. Kljun, M. Anko, K. Traven, M. Sinreih, Ž. Ude, E. E. Codina, J. Stojan, T. Lanišnik Rižner, I. Turel, *Dalton Trans.* **2016**, *45*, 11791 – 11800.

[19] a) W. Kandioller, A. Kurzwernhart, M. Hanif, S. M. Meier, H. Henke, B. K. Keppler, C. G. Hartinger, *J. Organomet. Chem.* **2011**, *696*, 999 – 1010; b) E. A. Enyedy, E. Sija, T. Jakusch, C. G. Hartinger, W. Kandioller, B. K. Keppler, T. Kiss, *J. Inorg. Biochem.* **2013**, *127*, 161 – 168.

[20] S. Ristovski, M. Uzelac, J. Kljun, T. Lipec, M. Uršič, Š. Zemljič Jokhadar, M. C. Žužek, T. Trobec, R. Frangež, K. Sepčić, I. Turel, *ChemMedChem* **2018**, *13*, 2166 – 2176.

[21] D. P. Martin, P. G. Blachly, J. A. McCammon, S. M. Cohen, *J. Med. Chem.* **2014**, *57*, 7126 – 7135.

[22] R. N. Adamek, C. V. Credille, B. L. Dick, S. M. Cohen, *J. Biol. Inorg. Chem.* **2018**, *23*, 1129 – 1138.

[23] F. Wang, A. Habtemariam, E. P. L. van der Geer, R. Fernandez, M. Melchart, R. J. Deeth, R. Aird, S. Guichard, F. P. A. Fabbiani, P. Lozano-Casal, I. D. H. Oswald, D. I. Jodrell, S. Parsons, P. J. Sadler, *Proc. Natl. Acad. Sci. USA* **2005**, *102*, 18269 – 18274.

[24] S. Seršen, J. Kljun, K. Kryeziu, R. Panchuk, B. Alte, W. Körner, P. Heffeter, W. Berger, I. Turel, *J. Med. Chem.* **2015**, *58*, 3984 – 3996.

[25] a) A. M. Pizarro, A. Habtemariam, P. J. Sadler, in *Activation Mechanisms for Organometallic Anticancer Complexes, Vol. 32* (Eds.: G. Jaouen, N. Metzler-Nolte), Springer-Verlag, Berlin, **2010**, pp. 21 – 56; b) W. H. Ang, E. Daldini, C. Scolaro, R. Scopelliti, L. Juillerat-Jeannerat, P. J. Dyson, *Inorg. Chem.* **2006**, *45*, 9006 – 9013.

[26] T. S. Lobana, R. Singh, *Polyhedron* **1995**, *14*, 907 – 912.

[27] A. E. Egger, C. G. Hartinger, A. K. Renfrew, P. J. Dyson, *J. Biol. Inorg. Chem.* **2010**, *15*, 919 – 927.

[28] C. J. Sherr, J. Bartek, *Annu. Rev. Cancer Biol.* **2017**, *1*, 41 – 57.

[29] R. G. Kenny, C. J. Marmion, *Chem. Rev.* **2019**, *119*, 1058 – 1137.

[30] I. Romero-Canelón, P. J. Sadler, *Inorg. Chem.* **2013**, *52*, 12276 – 12291.

[31] a) J. J. Soldevila-Barreda, I. Romero-Canelon, A. Habtemariam, P. J. Sadler, *Nat. Commun.* **2015**, *6*, 9; b) S. J. Dougan, A. Habtemariam, S. E. McHale, S. Parsons, P. J. Sadler, *Proc. Natl. Acad. Sci. USA* **2008**, *105*, 11628 – 11633.

[32] W. Davis, Z. Ronai, K. D. Tew, *J. Pharmacol. Exp. Ther.* **2001**, *296*, 1 – 6.

[33] R. E. Carraway, P. R. Dobner, *Biochim. Biophys. Acta Mol. Cell Res.* **2012**, *1823*, 544 – 557.

[34] F. Yang, Y. Zhang, H. Liang, *Int. J. Mol. Sci.* **2014**, *15*, 3580 – 3595.

[35] R. R. Ramsay, M. R. Popovic-Nikolic, K. Nikolic, E. Uliassi, M. L. Bolognesi, *Clin. Transl. Med.* **2018**, *7*, 14.

[36] X. Zhang, J. Lu, X. Ren, Y. Du, Y. Zheng, P. V. Ioannou, A. Holmgren, *Free Radical Biol. Med.* **2015**, *89*, 192 – 200.

[37] Y. Ouyang, Y. Peng, J. Li, A. Holmgren, J. Lu, *Metallomics* **2018**, *10*, 218 – 228.

[38] P. Mura, M. Camalli, A. Bindoli, F. Sorrentino, A. Casini, C. Gabbiani, M. Corsini, P. Zanello, M. P. Rigobello, L. Messori, *J. Med. Chem.* **2007**, *50*, 5871 – 5874.

[39] L. Oehninger, M. Stefanopoulou, H. Alborzinia, J. Schur, S. Ludewig, K. Namikawa, A. Muñoz-Castro, R. W. Köster, K. Baumann, S. Wölfl, W. S. Sheldrick, I. Ott, *Dalton Trans.* **2013**, *42*, 1657 – 1666.

[40] N. Y. S. Lam, D. Truong, H. Burmeister, M. V. Babak, H. U. Holtkamp, S. Movassaghi, D. M. Ayine-Tora, A. Zafar, M. Kubanik, L. Oehninger, T. Söhnel, J. Reynisson, S. M. F. Jamieson, C. Gaiddon, I. Ott, C. G. Hartinger, *Inorg. Chem.* **2018**, *57*, 14427 – 14434.

[41] A. Casini, C. Gabbiani, F. Sorrentino, M. P. Rigobello, A. Bindoli, T. J. Geldbach, A. Marrone, N. Re, C. G. Hartinger, P. J. Dyson, L. Messori, *J. Med. Chem.* **2008**, *51*, 6773 – 6781.

[42] L. Oehninger, H. Alborzinia, S. Ludewig, K. Baumann, S. Wölfl, I. Ott, *ChemMedChem* **2011**, *6*, 2142 – 2145.

[43] Z. Luo, L. Yu, F. Yang, Z. Zhao, B. Yu, H. Lai, K. H. Wong, S. M. Ngai, W. Zheng, T. Chen, *Metallomics* **2014**, *6*, 1480 – 1490.

[44] C. Schmidt, B. Karge, R. Misgeld, A. Prokop, R. Franke, M. Bronstrup, I. Ott, *Chem. Eur. J.* **2017**, *23*, 1869 – 1880.

[45] D. J. Daigle, T. J. Decuir, J. B. Robertson, D. J. Darensbourg in *1,3,5-Triaz-7-phosphatricyclo[3.3.1.1$^{3,7}$]decane and derivatives, Vol. 32* (Ed. M. Y. Darensbourg), Wiley, Hoboken, New Jersey, USA, **1998**, pp. 40 – 45.

[46] O. V. Dolomanov, L. J. Bourhis, R. J. Gildea, J. A. K. Howard, H. Puschmann, *J. Appl. Crystallogr.* **2009**, *42*, 339 – 341.

[47] G. Sheldrick, *Acta Crystallogr. Sect. A* **2015**, *71*, 3 – 8.

[48] A. Bolje, J. Košmrlj, *Org. Lett.* **2013**, *15*, 5084 – 5087.

[49] A. Jankowiak, P. Kaszynski, *J. Org. Chem.* **2009**, *74*, 7441 – 7448.

[50] J. Skiba, C. Schmidt, P. Lippmann, P. Ensslen, H. A. Wagenknecht, R. Czerwieniec, F. Brandl, I. Ott, T. Bernas, B. Krawczyk, D. Szczukocki, K. Kowalski, *Eur. J. Inorg. Chem.* **2017**, 297 – 305.

◄◄ These are not the final page numbers!

**Structural requirements of anticancer agents**: The first extended study of organoruthenium(II)-pyrithionato compounds has been conducted to explore the influence of minor structural alterations on their anticancer activity. To obtain the full potential of these compounds and to achieve all of the desired anticancer properties, the organic thiohydroxamic ligand must be bound to the ruthenium scaffold with labile chloride (see graphic).
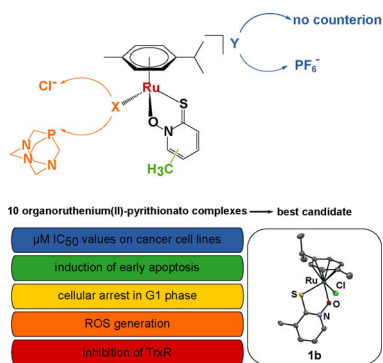
■ **Anticancer Agents**

*J. Kladnik, J. Kljun, H. Burmeister, I. Ott, I. Romero-Canelón, I. Turel\**

■■ – ■■

**Towards Identification of Essential Structural Elements of Organoruthenium(II)-Pyrithionato Complexes for Anticancer Activity**

## These are not the final page numbers! ↗↗